

Study the effect of discontinuity adaptive MRF models in fuzzy based classifier

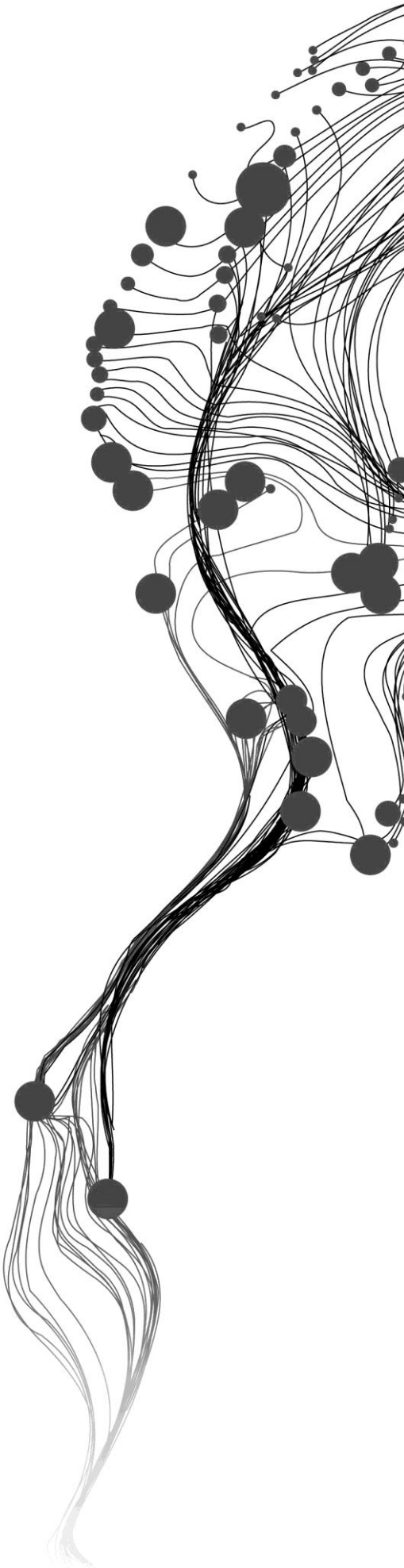
MRINAL SINGHA

March, 2013

SUPERVISORS:

Dr. Anil Kumar, IIRS

Prof. Dr. Ir. Alfred Stein, ITC



Study the effect of discontinuity adaptive MRF models in fuzzy based classifier

MRINAL SINGHA

Enschede, The Netherlands, March, 2013

Thesis submitted to the Faculty of Geo-Information Science and Earth Observation of the University of Twente in partial fulfilment of the requirements for the degree of Master of Science in Geo-information Science and Earth Observation.
Specialization: Geoinformatics

SUPERVISORS:

Dr. Anil Kumar, IIRS

Prof. Dr. Ir. Alfred Stein, ITC

THESIS ASSESSMENT BOARD:

Chair: Prof. George Vosselman

ITC professor: Prof. Dr. Ir. Alfred Stein

First supervisor (IIRS): Dr. Anil Kumar

Second supervisor (ITC): Prof. Dr. Ir. Alfred Stein

External examiner: Dr. Debashish Chaudhuri (Scientist, DEAL)

DISCLAIMER

This document describes work undertaken as part of a programme of study at the Faculty of Geo-information Science and Earth Observation of the University of Twente. All views and opinions expressed therein remain the sole responsibility of the author, and do not necessarily represent those of the Faculty.

Abstract

Presently wide ranges of remotely sensed data are available from earth observation satellites. These datasets are very useful to prepare land use/ land cover maps using different image processing techniques. Image classification is one way to produce these land use/ land cover maps. Due to continuous nature of real world phenomena, the image classification to map land cover classes is a challenge as well as presence of mixed pixels decreases the efficiency of image classification. Fuzzy classification technique such as fuzzy c-means (FCM) can be used to handle mixed pixels. Although FCM has the advantage of classifying mixed pixels by assigning membership value, it does not incorporate spatial contextual information of an image. Use of context eliminates the problem of isolated pixels and improves the classification accuracy.

In this research work a contextual FCM classifier was developed by using MRF models. Smoothness prior and four discontinuity adaptive MRF models have been used to incorporate contextual information with FCM classifier. The developed discontinuity adaptive contextual FCM classifier has been tested both on coarse and medium resolution dataset i.e. AWiFS and LISS-III of Resourcesat-1 and Resourcesat-2 with spatial resolution of 60 m and 20m respectively. Finer resolution LISS-IV image fraction outputs were used as a reference for assessing the accuracy of soft classified output of AWiFS and LISS-III image using an image to image based accuracy assessment technique.

The results of FCM, FCM-S and the FCM DA-MRF models were compared using fuzzy error matrix (FERM), the classification accuracy of FCM DA-MRF were improved by 0.5% to 5% and 1.5% to 6% respectively in comparison to FCM and FCM-S classifiers.

This study explored the applicability of discontinuity adaptive MRF models for incorporation of spatial contextual information. While observing the fuzzy accuracy measure (FERM) it was found that the FCM DA-MRF (H3) performs better than the other FCM DA-MRF models. It has been observed that the discontinuity adaptive MRF models (DA-MRF) improves the overall classification accuracy as well as preserves the edges at boundaries and generates the spectrally and spatially consistent classified output.

Key words: Fuzzy c-means, Contextual, Markov Random field, Discontinuity adaptive, Edge preservation, Fuzzy error matrix (FERM).

Acknowledgements

This research would not have completed without the help, support, comments and advices from my ITC supervisor, Prof. Dr. Alfred Stein. I would like to express my sincere gratitude for his guidance, suggestions and recommendations throughout the research period.

I acknowledge and express my deepest sense of gratitude to my IIRS supervisor Dr. Anil Kumar for his constant support, guidance and continuous encouragement. I highly appreciate his technical comments, suggestions and criticism during the progress of this research work. It is a great privilege for me to be your student. Thank you so much!

I would like to thank Dr. Y.V.N. Krishna Murthy, Director IIRS; Faculty of Geoinformatics division, Dr. S.K Shrivastav, Shri. P.L.N Raju, for all the supports and guidance provided by them.

I want to thank my parents for their unconditional love and support during my studies in IIRS. Without them I would not have gone this far.

I would also like to thank all my dear friends and classmates *Dipu, Anukesh, Ankur, Jayson, Sai, Shankar, Paji, Pavan, Hemanth, Ravi, Chetan and Bhavya* for their encouragement. Without them I would not have completed my study at IIRS.

A warm thanks to *Dipima, Sharath and Sangeeta* as they have tried to improve me in some way or other throughout these eighteen months in IIRS.

Mrinal Singha

Table of contents

List of figures.....	v
List of tables.....	vii
1. Introduction.....	9
1.1. Background	9
1.2. Problem statement	10
1.3. Research objectives	10
1.4. Research questions	10
1.5. Research set up	11
1.6. Structure of the thesis	12
2. Literature Review.....	13
2.1. Fuzzy c-Means clustering.....	13
2.2. Markov Random Field.....	14
2.3. Discontinuity Adaptive MRF models and over smoothing.....	15
2.4. Accuracy measure and validation.....	16
3. Markov Random Field in discontinuity adaptive contextual image classification	17
3.1. Markov Random field.....	17
3.2. Neighborhood System.....	18
3.3. Gibbs Random field.....	19
3.4. MRF-GRF Equivalence.....	20
3.5. Prior energy	20
3.6. Smoothness prior	20
3.7. Discontinuity Adaptive priors	21
3.8. Maximum A Posterior Solution (MAP)	23
3.9. Formulation of FCM Objective function to incorporate contextual information	24
3.10. Simulated Annealing and Gibbs sampling algorithm.....	26
3.11. Parameters to be estimated	26
3.12. Mean and variance method to verify edge preservation.....	27
3.13. Methods adopted for accuracy assessment.....	28
4. Study area and Data used	31
4.1. Study area.....	31
4.2. Data used.....	33
4.3. Pre-processing of the data.....	34

4.4.	Generation of reference dataset	36
5.	Results	38
5.1.	Estimated parameter	38
5.2.	Results of FCM Classification	41
5.3.	Contextual classification results for coarser resolution dataset	45
5.4.	Contextual classification results for medium resolution dataset	50
5.5.	Performance of FCM-S for untrained classes	52
5.6.	Performance of FCM DA-MRF for untrained classes	53
5.7.	Entropy measure of classified output.....	55
6.	Discussion.....	56
7.	Conclusion and recommendations.....	59
7.1.	Conclusion.....	59
7.2.	Recommendations.....	61
	List of references	62
	Appendix A.....	65
	Appendix B.....	66
	Appendix C.....	68
	Appendix D	90

List of figures

Figure 1.1: General methodology adopted for this study	11
Figure 3.1: Neighbourhood system of different order for pixel r [6]. (a) First-order (b) Second-order (c) Fifth-order	18
Figure 3.2: Patterns of the cliques with first-order and second-order neighbourhood system	19
Figure 3.3: Qualitative shape of four DA functions [7].....	23
Figure 3.4: Method to verify edge preservation.....	28
Figure 4.1: Location of Sitarganj study area (<i>source</i> : Google Earth, accessed on 11 th Jan 2013)/ LISS-IV (Resourcesat-2)/ Field photographs.....	32
Figure 4.2: Comparing finer resolution image with coarser resolution image	35
Figure 5.1: Estimation of Initial Temperature T_0	38
Figure 5.2: Estimation of λ and β	39
Figure 5.3: Field photographs of study area.....	42
Figure 5.4: AWiFS and LISS-III images of study area	43
Figure 5.5: FCM classification output of AWiFS image from Resourcesat-1	44
Figure 5.6: FCM classification output of AWiFS image from Resourcesat-2.....	44
Figure 5.7: Comparison of FERM overall accuracy obtained by different classifiers for AWiFS image from Resourcesat-1	45
Figure 5.8: Fraction images generated from contextual FCM classification for AWiFS image from Resourcesat-1. (a) FCM-S (b) FCM DA-MRF (H1) (c) FCM DA-MRF (H2) (d) FCM DA-MRF (H3) (e) FCM DA-MRF (H4) , (1) Agriculture field with crop (2) Dry agriculture field without crop (3) Eucalyptus plantation (4) Moist agriculture field without crop (5) Sal forest (6) Water ..	47
Figure 5.9: Comparison of FERM overall accuracy obtained by different classifiers for AWiFS image from Resourcesat-2	49
Figure 5.10: Comparison of FERM overall accuracy obtained by different classifiers for LISS-III image from Resourcesat-1	50
Figure 5.11: Comparison of FERM overall accuracy obtained by different classifiers for LISS-III image from Resourcesat-2	51
Figure 5.12: Comparison of average user's accuracy of different classifiers for LISS-III image from Resourcesat-1	54

List of tables

Table 4.1: Images used for this research work.....	33
Table 4.2: Sensors specification of Resourcesat-1(R1) and Resourcesat-2(R2) (<i>source</i> : www.isro.org , accessed on 8 th Jan 2013).....	34
Table 5.1: Verification of edge preservation for λ values.....	40
Table 5.2: Verification of edge preservation for β values.....	40
Table 5.3: Verification of edge preservation for γ values	40
Table 5.4: optimized parameter value	41
Table 5.5: Land cover classes for the study area	42
Table 5.6: Verify edge preservation for AWiFS from Resourcesat-1	48
Table 5.7: Verify edge preservation for AWiFS from Resourcesat-2.....	49
Table 5.8: Verify edge preservation for LISS-III from Resourcesat-1	51
Table 5.9: Verify edge preservation for LISS-III from Resourcesat-2.....	52
Table 5.10: Accuracy assessment report (FERM) of FCM-S classification for LISS-III image of Resourcesat-1 with LISS-IV as a reference image while class 2 (Agriculture field with crop) was not considered	53
Table 5.11: Accuracy assessment report (FERM) of FCM DA-MRF (H3) classification for LISS-III image of Resourcesat-1 with LISS-IV as a reference image while class 2 (Agriculture field with crop) was not considered	54
Table 5.12: Comparison of entropy values of classified output.....	55
Table C 1: Accuracy assessment report of FCM classification for AWiFS image of Resourcesat-1 with LISS-IV as a reference image	68
Table C 2: Accuracy assessment report of FCM classification for AWiFS image of Resourcesat-2 with LISS-IV as a reference image	69
Table C 3: Accuracy assessment report of FCM-S classification for AWiFS image of Resourcesat-1 with LISS-IV as a reference image	70
Table C 4: Accuracy assessment report of FCM DA-MRF (H1) classification for AWiFS image of Resourcesat-1 with LISS-IV as a reference image.....	71
Table C 5: Accuracy assessment report of FCM DA-MRF (H2) classification for AWiFS image of Resourcesat-1 with LISS-IV as a reference image.....	72
Table C 6: Accuracy assessment report of FCM DA-MRF (H3) classification for AWiFS image of Resourcesat-1 with LISS-IV as a reference image.....	73
Table C 7: Accuracy assessment report of FCM DA-MRF (H4) classification for AWiFS image of Resourcesat-1 with LISS-IV as a reference image.....	74
Table C 8: Accuracy assessment report of FCM-S classification for AWiFS image of Resourcesat-2 with LISS-IV as a reference image.....	75
Table C 9: Accuracy assessment report of FCM DA-MRF (H1) classification for AWiFS image of Resourcesat-2 with LISS-IV as a reference image.....	76
Table C 10: Accuracy assessment report of FCM DA-MRF (H2) classification for AWiFS image of Resourcesat-2 with LISS-IV as a reference image.....	77

Table C 11: Accuracy assessment report of FCM DA-MRF (H3) classification for AWiFS image of Resourcesat-2 with LISS-IV as a reference image.....	78
Table C 12: Accuracy assessment report of FCM DA-MRF (H4) classification for AWiFS image of Resourcesat-2 with LISS-IV as a reference image.....	79
Table C 13: Accuracy assessment report of FCM-S classification for LISS-III image of Resourcesat-1 with LISS-IV as a reference image.....	80
Table C 14: Accuracy assessment report of FCM DA-MRF (H1) classification for LISS-III image of Resourcesat-1 with LISS-IV as a reference image.....	81
Table C 15: Accuracy assessment report of FCM DA-MRF (H2) classification for LISS-III image of Resourcesat-1 with LISS-IV as a reference image.....	82
Table C 16: Accuracy assessment report of FCM DA-MRF (H3) classification for LISS-III image of Resourcesat-1 with LISS-IV as a reference image.....	83
Table C 17: Accuracy assessment report of FCM DA-MRF (H4) classification for LISS-III image of Resourcesat-1 with LISS-IV as a reference image.....	84
Table C 18: Accuracy assessment report of FCM-S classification for LISS-III image of Resourcesat-2 with LISS-IV as a reference image.....	85
Table C 19: Accuracy assessment report of FCM DA-MRF (H1) classification for LISS-III image of Resourcesat-2 with LISS-IV as a reference image.....	86
Table C 20: Accuracy assessment report of FCM DA-MRF (H2) classification for LISS-III image of Resourcesat-2 with LISS-IV as a reference image.....	87
Table C 21: Accuracy assessment report of FCM DA-MRF (H3) classification for LISS-III image of Resourcesat-2 with LISS-IV as a reference image.....	88
Table C 22: Accuracy assessment report of FCM DA-MRF (H4) classification for LISS-III image of Resourcesat-2 with LISS-IV as a reference image.....	89

1. Introduction

1.1. Background

The number of remote sensing satellites with coarse to fine resolution launched worldwide have been increased. These satellites provide a large amount of remote sensing images of the earth resources. Such satellite images contain wealth of information which play a significant role in the development and planning of natural resources.

Satellite images are further analyzed to prepare land use/land cover maps using digital image processing techniques in a fast and economic way. These land use/land cover maps are the important input for any kind of development and conservation projects. Image classification is important to produce these land use/land cover maps. In image classification, pixels representing similar objects are grouped together to form land cover classes or clusters.

The most commonly used classifiers are the hard classifiers. They assume that a pixel takes either 1 or 0 memberships to a single class and the pixel is considered as a pure pixel. The pixels have membership value equal to 0 for the classes to which they do not belong and membership value equal to 1 for the class to which they belong. For actual data, however, a single pixel may contain more than one class, such as a combination of, forest, water, bare soil and grass. This happens because real world phenomena change gradually from one class to another as well as due to compatibility of spatial resolution with class size forms mixed pixels. Therefore at the boundaries of different classes uncertainty increases and fuzziness or vagueness occurs.

To overcome the problem of multiple classes at the boundaries in 1965, L.A Zadeh introduced fuzzy set theory which is based upon uncertainty and vagueness [1]. Fuzzy sets can have the membership values between 0 and 1 also. The degree of the membership value can be assigned for a pixel which handles the problem of having multiple classes in a pixel. This means that a pixel is assigned to more than one cluster. Fuzzy c-means clustering (FCM) [2] is one of the popular fuzzy based soft classification technique which takes care of uncertainty and vagueness in class definition.

Fuzzy c-means clustering (FCM) introduced by Bezdek [2] is a well-known unsupervised iterative algorithm to calculate the fuzzy membership grades. Fuzzy c-means clustering finds the cluster center based on the minimization of an objective function. The objective function of fuzzy c-means clustering (FCM) clusters the patterns in a similar group which have highest similarity. Standard fuzzy c-means clustering does not incorporate spatial contextual information of the pixels into its classifying algorithm; it considers only the spectral information of the pixels. More detail of fuzzy c-means clustering has been provided in appendix A.

To incorporate spatial contextual information Markov Random Field (MRF) is being widely used [3],[4],[5]. MRF theory is able to model context dependent entities such as pixels or correlated features in a convenient and consistent way [5]. Spatial context implies the presence of correlation of class labels within neighbouring pixels [4]. The actual geographical phenomenon lies in context to others. For example vegetation has a high probability to have the same vegetation pixels as its neighbours. So the isolated pixels exist rarely. Use of context eliminates the problem of isolated

pixels [6]. In this research work, MRF model has been used to develop the contextual based supervised FCM classifier.

To model the context it is important to select the MRF models carefully for accurate results. The MRF models also called as MRF priors and regularizers. The various MRF models are standard regularization model, weak string and membrane model, line process model, and discontinuity adaptive (DA) MRF models. In this research work standard regularization model (smoothness prior) and discontinuity adaptive (DA) MRF models (edge preserving priors) have been studied for smoothing effect as well as edge preserving effect in an image.

1.2. Problem statement

MRF uses smoothness prior models and calculates prior energy using prior probabilities to model the smoothness in the images [6]. This applies a contextual concept of smoothness, in which it assumes uniform smoothness everywhere. If discontinuities are overlooked (e.g. at boundaries), however, MRF leads to over-smoothing, loss of information and hence to less accurate results [5],[7]. Smoothness prior can be used to compensate for this, as these can preserve the edges, as was mentioned by Li [5]. This leads to the use of discontinuity adaptive (DA) models [7] or adaptive neighbourhoods [8] that can be used to overcome the problems of discontinuity. This research work continues along these lines and proposes to study the effect of various discontinuity adaptive MRF models in a fuzzy c-means classifier.

1.3. Research objectives

The main objective of this study has been to incorporate spatial contextual information in a fuzzy c-means classifier, using discontinuity adaptive MRF models. The specific objectives were;

1. To incorporate spatial contextual information in fuzzy c-means classifier using discontinuity adaptive MRF models.
2. To study of four discontinuity adaptive MRF models for fuzzy c-means classification.
3. To develop a fuzzy c-means classifier incorporating spatial contextual information using discontinuity adaptive MRF models to preserve edges.
4. To evaluate the performance of the fuzzy c-means classification after applying discontinuity adaptive MRF models in the case of untrained classes.

1.4. Research questions

In order to meet the solutions of the above mentioned objective the following questions needed to be answered.

1. How can spatial contextual information be incorporated into an FCM classification when DA-MRF models are to be used?
2. How should the FCM objective function be formulated to allow incorporation of context using DA-MRF models?
3. Which is a best DA-MRF model for a specific FCM?
4. What is the accuracy of the FCM adjusted with DA-MRF as compared to FCM?
5. How much does an FCM DA-MRF model improve in terms of classification accuracy as compared to FCM with a smoothness prior MRF model?
6. How does FCM DA-MRF perform in case of untrained classes?

1.5. Research set up

To obtain the research objective and to answer the research questions, the following methodology showed in figure 1.1 has been adopted. The complete methodology for this study can be divided into three stages.

1. FCM-MRF model: Spatial contextual information has been incorporated with FCM using smoothness prior (FCM-S) and using discontinuity adaptive MRF models (FCM DA-MRF).
2. Classification: Classification of coarse and medium resolution images have been performed by FCM, FCM-S and FCM DA-MRF separately.
3. Accuracy measure: Accuracy assessment of classified fraction images using Fuzzy Error Matrix (FERM) [9] .

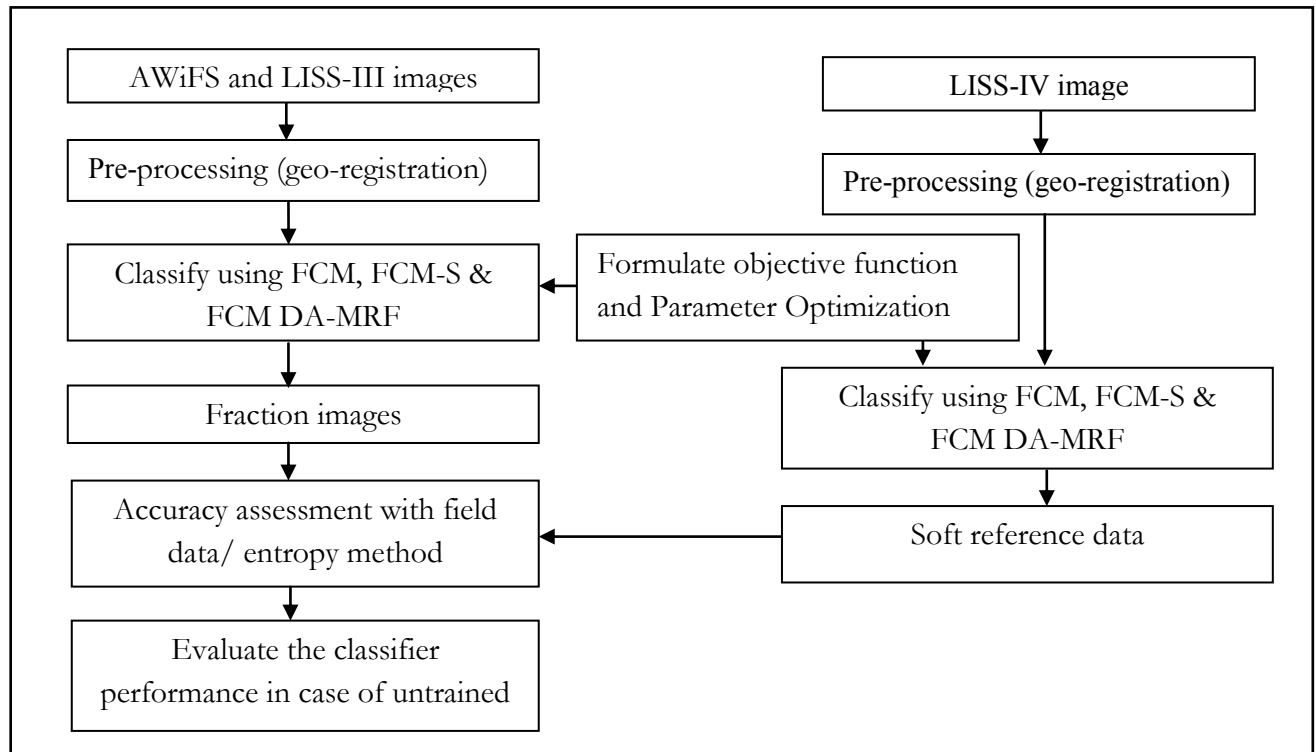


Figure 1.1: General methodology adopted for this study

1.6. Structure of the thesis

This thesis contains seven chapters. The first chapter covers background information of the research topic with the problem statement, research objectives, research questions and research setup. In second chapter previous researches done by others have been reviewed. Third chapter includes the theory of Markov random field in discontinuity adaptive contextual image classification. Fourth chapter describes the study area and the data used. Fifth chapter presents the results of this research work. Chapter sixth discusses about the obtained results. Last chapter includes the conclusion and recommendation for future research.

2. Literature Review

In this chapter, research work done by various researchers in past has been discussed related to Fuzzy c-Means clustering (FCM); Markov Random Field (MRF); Discontinuity adaptive MRF models and over smoothing. The accuracy measure and validation of fuzzy based classifiers were also reviewed.

2.1. Fuzzy c-Means clustering

Wang [10] used supervised FCM classification to classify Landsat MSS and TM data. FCM classifier was able to identify the land cover classes from the mixed pixels. The overall classification accuracy of 5.11% had been improved as compare to the maximum likelihood classifier.

Zhang and Foody [11] tested the FCM on SPOT HRV and Landsat TM. It was observed that in case of sub-urban land cover mapping fuzzy classification provided more appropriate classification results. The 20% improvement in accuracy had been observed in comparison to the hard classifier.

Okeke and Karnieli [12] applied FCM classification on aerial photograph to find out quantitative changes in trees and other vegetation types. Combined supervised and unsupervised FCM algorithm was used for the classification of aerial photographs for change analysis. In this work for output evaluation Fuzzy Error Matrix (FERM) was used whereas ground reference data were not available and the fuzzy overall accuracy for all the datasets were more than 85%.

Kannan *et al.* [13] used FCM for segmentation of a synthetic MRI image while incorporating noise clustering concept into the entropy based FCM. This FCM method was able to deal with the uncertainty presents in the dataset during the segmentation of MR images. The accuracy of the proposed FCM with noise clustering method was exceeded that of the standard FCM.

Lucas *et al.* [14] used FCM and linear mixture model on the airborne imaging spectrometer (CASI) images to map the habitat of costal dune ecosystem. Spectral unmixing of CASI image was done by linear mixture model and fuzzy membership function. Both the classifier techniques were able to map the sand and vegetation successfully at the sub-pixel level. It was concluded that FCM and linear mixture model could be useful to map the land cover class at sub-pixel level.

Foody [15] has applied FCM and fuzzy neuron network (ANN) on airborne thematic mapper (ATM) data to classify land cover classes. In FCM classification it was found that with $m=2.0$ (fuzzy weight parameter) provided high accuracy for maximum cases. Finally in this work it was concluded that in comparison to hard classification approach fuzzy classification gave higher accuracy for land cover classification.

In another work Zhang and Foody [16] applied FCM and ANN technique to classify sub-urban land cover from Landsat TM data. The improvement in classification accuracy of 5.0 % to 6.6% had been noticed for the fuzzy classifier in comparison to partially-fuzzy approach.

In a recent study by Wang *et al.* [17] FCM was used with Ant colony optimization algorithm (ACA) for segmentation of remote sensing image. ACA-FCM could enhance the speed of segmentation, while reducing the noise on the image. The surface features in the image were well segmented in comparison to Log operator and Log operator with canny operator.

Bastin [18] showed that FCM gave better sub-pixel land-cover classification on aggregated TM image. In this work comparative study was conducted among FCM, linear mixture modelling and maximum likelihood classifier while classifying aggregated Landsat TM image.

Ibrahim *et al.* [19] showed the need of mixed pixel image classification to generate more accurate land cover classes. In this work the maximum likelihood classifier (MLC), Fuzzy c-means classifier (FCM) and possibilistic c-means classifier (PCM) had been studied in presence of uncertainties and found that PCM gave more accurate results followed by FCM. The accuracy obtained from the error matrix, were 66.8%, 69.2%, 70.0% for MLC, FCM, PCM respectively.

2.2. Markov Random Field

Geman and Gema [3] did maximum a priori (MAP) estimation as statistical criterion using simulated annealing and Gibbs Sampler for MRF model based image restorations. It was found improved restorations at low signal-to-noise ratio. It explains the equivalence between Gibbs distribution and Markov random field (MRF). The restoration was performed using the simulated annealing theorem which convergence to the global maxima of the posterior distribution. Similar simulated annealing algorithm was used in this research work to find out the global posterior energy without sticking in a local minimum.

Solberg *et al.* [4] used MRF model to include context for multisource satellite images. It was found that MRF model can model spatial class dependencies as well as temporal class dependencies. MRF model achieved 2% higher classification accuracy when same set of images used for the two different models. Finally it was concluded that MRF model provide better results for classification of multisource satellite images.

Pham [20] included spatial constraints using MRF model on the membership function of FCM for image segmentation and it was named as Robust Fuzzy C-means or RFCM algorithm. The value of smoothness controller β was obtained by the penalty function or objective function. In this work the new formulation of FCM was applied on Magnetic Resonance Images (MRI) of brain and it was found that RFCM to be more robust to noise than FCM classification. The comparative results calculated by misclassified rate (MCR) was 14.14% for FCM and for RFCM it was 0.52%.

Melgani and Serpico [21] used MRF model to integrate contextual and spatio-temporal information for the classification of Landsat TM and ERS-1 SAR images. In this work it was proposed a “mutual” approach for image classification. In this study it was found that proposed “mutual” method shows improvement of 1% to 3% in classification accuracy as compared to reference MRF model based classifier.

Tso and Olsen [22] have used contextual and multiscale fuzzy line process for classification of IKONOS image. MRF model was used for contextual information, wavelet and fuzzy fusion process to extract line features. The accuracy was improved to 13%, while using MRF model based contextual and edge information image classification.

Kasetkasem *et al.* [23] used MRF model for super-resolution land cover mapping. In this work the proposed MRF model based approach was applied on IKONOS MSS and Landsat ETM+ images. The results showed a significant improvement in accuracy of land cover maps over that obtained from Land cover mapping at sub pixel scales using Linear Optimization approach given by Verhoeve and wulf (2002).

Moser and Serpico [24] proposed contextual support vector machines (SVM) classifier based on MRF model. To minimize the execution time and to automatically tune its input parameters hierarchical clustering and parameter optimization algorithm was also integrated with SVM. The developed method was applied on SAR and multispectral high resolution images. The overall accuracy was 0.9392 and 0.9898 for traditional SVM and proposed MRF model based SVM respectively.

2.3. Discontinuity Adaptive MRF models and over smoothing

Li [7],[25] introduced discontinuity adaptive (DA) MRF models to avoid over smoothing. The major differences among different discontinuity adaptive MRF models lies how they interact with their neighboring points and control the smoothing strength. The DA models works in the principle that whenever a discontinuity takes place it minimize the smoothing strength accordingly.

Smits and Dellepiane [26] used discontinuity adaptive MRF model combined with gamma distribution for segmentation of synthetic aperture radar (SAR) images. The developed method was able to preserve the fine structure and borders of the images.

In another work by Smits and Dellepiane [27] used MRF model combining with adaptive neighbourhoods segmentation of synthetic aperture radar (SAR) images. It was found that MRF model segmentation approach with adaptive neighbourhood can preserve the small features in better way.

Homen *et al.* [28] used MRF model for super resolution image reconstruction using Iterated conditional modes (ICM) algorithm to find maximum a posterior (MAP) solution. Discontinuity adaptive framework was used to avoid over smoothness of MAP-MRF formulations for sixteen low-resolution (LR) images.

Kang and Roh [29] presented a new method to increase the performance of edge-preserving image smoothing of MRF function by the parameter tuning. The method was based on an automatic control of smoothing strength in discontinuity adaptive MRF function from discontinuities of image intensity. An algorithm was proposed which used parameter modification to increase the piecewise smoothness of images in a discontinuity adaptive (DA) MRF modelling. The proposed method was well preserved the object boundaries in comparison to conventional DA smoothing.

Debayle and Pinoli [30] used adaptive neighbourhood image processing on a real human retina image. The used adaptive neighbourhood approach was context-dependent analysis which considers the radiometric as well as geometric properties of the image.

More details on MRF based images analysis are available in Li [5]. This book provides the reference to theories, methodologies and recent developments in computer vision problems based on MRF model. The various problems were discussed in low and high level vision problem within the MAP-MRF framework. The details on discontinuity adaptive MRF models were also explained in Li [5].

2.4. Accuracy measure and validation

Accuracy assessment and validation of soft classification output is still a research area. In case of hard classification output error matrix and kappa coefficient have been widely used for accuracy measure but there are no such standard methods for soft classifiers output. Some researchers have hardened the soft classifiers output, but doing so it leads to loss of information [9]. To carry out the accuracy measure of the soft classified output, a modified error matrix i.e. FERM (Fuzzy Error Matrix) has been proposed by the Binaghi *et al.*[9] and SCM (Sub-pixel confusion-uncertainty matrix) has been proposed by Silvan and Wang [31]. This fuzzy error matrix is used to derive the accuracy of soft classifier when the output as fraction images. FERM is used the same as the traditional error matrix but the main difference is that FERM uses fractional images to measure the accuracy and the values in FERM are real number (integers in conventional error matrix). The overlap between classified and reference datasets is calculated by using single operators like Min, Least and Prod or composite operators like MIN-MIN and MIN-LEAST and MIN-PROD [31], [32].

Dehghan and Ghassemian [33] had given entropy measure to assess the accuracy of the classified output by measuring the uncertainty in the results. The entropy gives the absolute measure of uncertainty. This is called absolute because it does not take any reference data to measure the uncertainty. Entropy is the indirect method of accuracy assessment. Entropy method is used for accuracy measure when there are no references data available for accuracy measurement. The higher entropy implies higher uncertainty and vice-versa in class identification on classified output. The advantage of entropy measure for accuracy assessment was also proven by Kumar and Dadhwal [34].

3. Markov Random Field in discontinuity adaptive contextual image classification

This chapter describes the fundamental concepts and theory behind the Markov Random Field (MRF) and the developed, discontinuity adaptive contextual image classifier. It also covers the methods adopted for accuracy assessment.

3.1. Markov Random field

In remote sensing image analysis Bayesian theory has a strong influence on statistical modelling of images. Bayesian classification consists of prior and conditional probability density functions (p.d.f). By using these functions, a classification can be obtained in terms of maximum posterior (MAP) criteria [6]. In practice, problems are there to use MAP estimates. One of the difficulties is that prior information of the data distribution may not always available. So it is necessary to use alternative criteria instead of MAP. Maximum likelihood (ML) criteria can be used if the knowledge of data distribution is available without the prior information of data. A maximum likelihood criterion is being widely used in remote sensing image classification. Most classification follows Gaussian distribution to model class-conditional p.d.f., but prior p.d.f., is not used generally. Classification results can be improved if MAP estimation is done by modelling of prior p.d.f and the class-conditional p.d.f. For modelling of prior probability context is one assumption [6].

Proper use of context can improve the classification accuracy [4], [35],[36],[22]. Context is important in visual image interpretation. It can be obtained from spectral, spatial or from temporal attributes [6], [4]. Context generates the smooth image classification pattern. Use of context eliminates the possible ambiguities; recover missing information and correction of errors [36]. In contextual image classification the pixels are not treated as isolation but as it has a statistical dependence with its neighbour pixels [6]. In this thesis spatial contextual information has been exploited for image classification.

Markov Random Field (MRF) is a useful tool for modelling the contextual information and widely used to image segmentation and restoration problems [37],[3]. It is also a branch of probability theory that characterize the spatial or contextual relationship of physical phenomena [6].

MRF theory and its formulations described here were adopted from T'so and Mather [6].

Let, $d = \{d_1, d_2, \dots, d_n\}$ denote a set of random variables, can be defined on the set of S containing n number of sites (pixels) in which each random variable takes a label (membership values) for class L , here the family d is called random filed. The set S is equivalent to an image containing n pixels; d is a set of pixel DN values, and the label set L depends on user defined application, i.e. $L = \{ \text{water, forest, agriculture land, fallow land} \}$. Based on the definition of random of random field, the configuration w for set S as $w = \{d_1 = w_1, d_2 = w_2, \dots, d_n = w_n\}$ where $w_r \in L (1 \leq r \leq n)$. The notation of w can be simplified to $w = \{w_1, w_2, \dots, w_n\}$. A random field, with respect to a neighbourhood system is a Markov Random field if only if its probability density function satisfies the following three properties [6].

Positivity: $P(w) > 0$, for every possible configuration of w . It states that, it has a non-zero probability and $P(w)$ is the probability of given dataset w .

Markovianity: $P(w_r | w_{s-r}) = P(w_r | w_{N_r})$, it defines the neighbourhood system. This property means that, membership value of pixel r is only dependent on its neighbouring pixels.

Homogeneity: $P(w_r | w_{N_r})$ is the same for all pixels r , this property specifies the probability for the label of all pixels is dependent on neighbouring pixels regardless of the pixel location.

An MRF also satisfy other property such as isotropy. This is the direction independence property among the neighbouring pixels. It means that the neighbouring pixels surrounding a pixel r have the same contributing effect to the labelling of pixel r [6].

3.2. Neighborhood System

In image analysis to define neighbourhood, there is a system that takes some surrounding pixels as a neighbour. Usually neighbourhood system used in image analysis defines the first-order neighbourhood that contains four pixels sharing a side with the central pixel, as shown in figure 3.1(a). Second-order neighbourhood contains four pixels having corner boundaries with the pixel of interest [6], as shown in figure 3.1(b). Higher order neighbourhood system can be formed in a similar fashion. In figure 3.1(c) neighbourhood system order up to five is shown. In this thesis only the second-order neighbourhood system is considered.

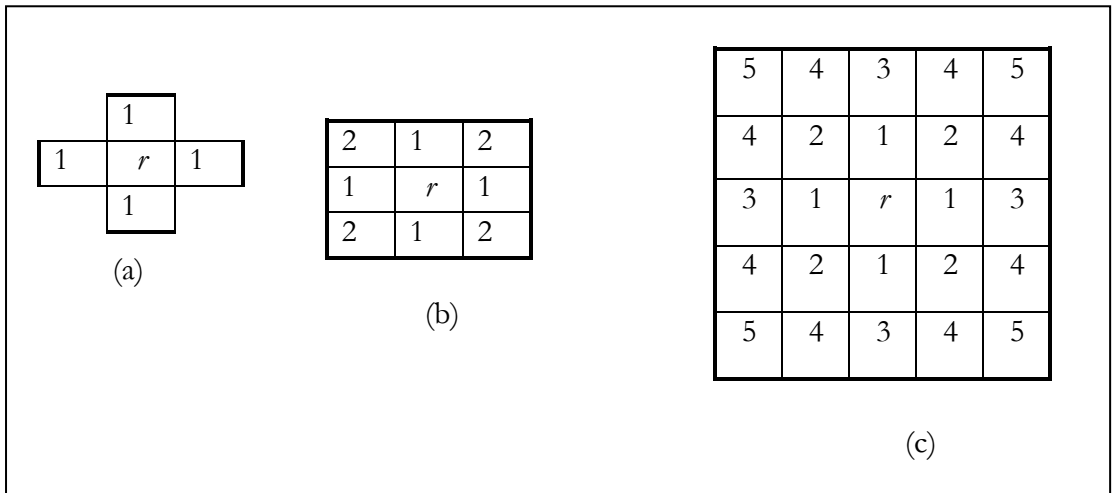


Figure 3.1: Neighbourhood system of different order for pixel r [6]. (a) First-order (b) Second-order (c) Fifth-order

3.3. Gibbs Random field

Gibbs random field (GRF) defines a global model for an image. GRF provides a global model of an image by specifying a p.d.f as in equation (3.1) [6].

$$P(w) = \frac{1}{Z} \exp\left(-\frac{U(w)}{T}\right) \quad \text{Equation (3.1)}$$

where, $P(w)$ is the probability of w , $U(w)$ is the energy function, T is a constant termed temperature, and Z is the partition function, it can be expressed as equation (3.2).

$$Z = \sum \exp\left(-\frac{U(w)}{T}\right) \quad \text{Equation (3.2)}$$

In equation (3.2) Z is the sum of all possible combination of w . In case of an image all combinations of pixel values. In practice Z is not computable except for very simple cases. This difficulty in computation of Z complicates sampling and estimation problems [6]. From Equation (3.4) maximization of $P(w)$ is equivalent to minimization of the energy function $U(w)$ as equation (3.3).

$$U(w) = \sum_{c \in C} V_c(w) \quad \text{Equation (3.3)}$$

In equation (3.3) C is a clique. $C = C_1 \cup C_2 \cup C_3 \cup \dots$, is the collection of all possible cliques, C is a subset of image and within a clique all pairs of pixels are mutual neighbours. $V_c(w)$ is called the potential function with respect to clique C [6]. All possible collections of pixel for first-order and second-order cliques were shown in figure (3.2).

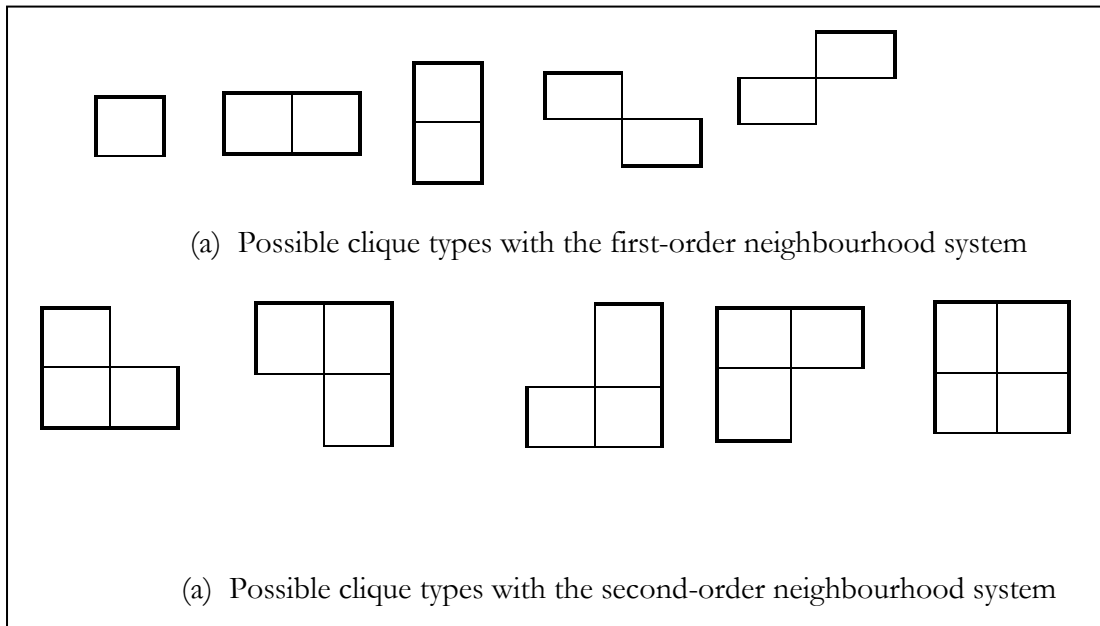


Figure 3.2: Patterns of the cliques with first-order and second-order neighbourhood system

As the order of neighbourhood system increases the number of cliques grows rapidly, so the computational complexity also increases. The energy function $U(w)$ in equation (3.3) can also be expanded in equation (3.4) [6].

$$U(w) = \sum_{\{r\} \in \mathcal{C}_1} V_1(w_r) + \sum_{\{r, r'\} \in \mathcal{C}_2} V_2(w_r, w_{r'}) + \sum_{\{r, r'', r'''\} \in \mathcal{C}_3} V_3(w_r, w_{r'}, w_{r''}) + \dots \text{Equation (3.4)}$$

where $\mathcal{C}_1, \mathcal{C}_2, \mathcal{C}_3$ represents a single-site, a pair-site, a triple-site and a quadratic-site clique respectively. In this study only \mathcal{C}_2 has been considered and it is the choice of second order neighbourhood system.

3.4. MRF-GRF Equivalence

An MRF describes in terms of local properties of an image whereas GRF describes global properties of an image. According to Hammersley-Clifford theorem there is an equivalence of GRF and MRF properties and a unique GRF exists for every MRF as long as the GRF is defined in terms of cliques on a neighbourhood system [6]. The proof of MRF-GRF equivalence can be found in Tso and Mather [6]. This equivalence provides a simple way to address MRF-based contextual image analysis problems.

3.5. Prior energy

The energy function represented by $U(w)$ is called as the prior energy. $U(w)$ from equation (3.4), provides the *prior knowledge* about the image. In image classification, smoothness assumption is usually adopted to model the prior information [6]. To model the prior energy several functions are available in the literature and they are known as smoothness prior. For example *Auto-models*, *Multi-level Logistic model*, *Auto-logistic model* or *Ising model* etc. [5], [6].

3.6. Smoothness prior

Smoothness is the generic constraint of context. It assumes that a physical property does not change abruptly [5]. In case of an image the DN values of the pixels do not change suddenly and present some coherence. This assumption of smoothness has been applied in early applications of vision problem [38], [39]. To compute image properties, the smoothness prior is the most popular prior assumption in low-level vision. Smoothness assumption is expressed as the prior probability or equivalently an energy term $U(f)$ [5]. The analytic regularization model provides a convenient platform for the study of smoothness prior [5]. Equation (3.5) defines the general form of these regularizers [7]:

$$U(f) = \sum_{n=1}^N U_n(f) = \sum_{n=1}^N \lambda_n \int_a^b g(f^{(n)}(x)) dx \quad \text{Equation (3.5)}$$

where, $U(f)$ is the prior energy and it is the smoothness term, $U_n(f)$ is the n^{th} order regularizer, N is the highest order to be considered and $\lambda_n \geq 0$ is a weighting factor. This regularizers model is based on Euler equation, so order of derivative is considered with boundary condition $f(a)$ and $f(b)$. The potential function $g(f^{(n)}(x))$ is dependent on irregularity in $f^{(n-1)}(x)$, and all the regularizers vary according to this potential function i.e. $g(f^{(n)}(x))$. In this thesis *standard regularizer* is used as smoothness prior. Standard regularizers take the pure quadratic form as given by equation (3.6);

$$g_q(\eta) = \eta^2 \quad \text{Equation (3.6)}$$

More irregularity in $f^{(n-1)}(x)$ increases $|f^n|$ and contributes to a higher energy i.e. $U(f)$. This standard regularization based smoothness prior has been used previously by [40],[41] with FCM and PCM classifier respectively. The disadvantages of this regularization model are [7]:

- (a) This considers constant interaction among neighboring points.
- (b) Smoothing strength is proportional to the derivative magnitudes $|f^n|$.

So this causes over-smoothing at discontinuities at which the derivative is infinite [7].

3.7. Discontinuity Adaptive priors

Smoothness assumption implies uniform smoothness everywhere [7]. But in a real image discontinuity occurs at the boundaries or at edges and the image itself is a piecewise discontinuous surface [5]. However improper use or applying smoothness homogeneously everywhere can lead to over smoothing and undesirable results, so it is important to take care of discontinuities while using smoothness priors [25], [5]. Hence in this thesis, discontinuity adaptive (DA) priors have been used to model the prior energy and to preserve the edges.

The fundamental difference among different regularizers lies how they interact with their neighbouring points and control the interaction [5]. The discontinuity adaptive smoothness models works in a principle that whenever a discontinuity occurs, the interaction should decrease.[5]. There are four possible choices available for the potential function i.e. $g(\eta)$ and is also termed as adaptive potential function (APF). The derivative of the APF is expressed as given in the equation (3.7).

$$g'(\eta) = 2\eta h(\eta) \quad \text{Equation (3.7)}$$

where, h is the interaction function, also called the *adaptive interaction function* (AIF). The smoothness strength depends on the shape of the AIF; it is determined by h_γ where γ is a parameter. The strength with which a regularizer performs smoothing is given in equation (3.8).

$$|g'(f')| = |2f'h(f')| \quad \text{Equation (3.8)}$$

where, $h(f'(x))$ determine the interaction between neighbouring pixels.

Working principle of DA priors:

The necessary condition for regularization model to be “discontinuity adaptive” [7] has been mentioned in equation (3.9):

$$\lim_{\eta \rightarrow \infty} |g'(\eta)| = \lim_{\eta \rightarrow \infty} |2\eta h(\eta)| = C \quad \text{Equation (3.9)}$$

where, $C \in [0, \infty]$ and it is a constant. The condition with $C = 0$ entirely disallow smoothing at discontinuities where $\eta \rightarrow \infty$. If $C > 0$ it allows bounded or limited smoothing. However for large $|\eta|$, the interaction $h(\eta)$ will be small and approaches 0 as $|\eta|$ goes to ∞ [5]. This way the DA model works.

The DA models used:

The four possible choices of DA models have been given by Li [5]. All the four DA models have been studied in this thesis. In equation (3.10) - (3.13) the DA models were mentioned.

$$g_{1\gamma}(\eta) = -\gamma e^{-\frac{\eta^2}{\gamma}} \quad \text{Equation (3.10)}$$

$$g_{2\gamma}(\eta) = -\frac{\gamma}{1 + \frac{\eta^2}{\gamma}} \quad \text{Equation (3.11)}$$

$$g_{3\gamma}(\eta) = \gamma \ln(1 + \frac{\eta^2}{\gamma}) \quad \text{Equation (3.12)}$$

$$g_{4\gamma}(\eta) = \gamma |\eta| - \gamma^2 \ln(1 + \frac{|\eta|}{\gamma}) \quad \text{Equation (3.13)}$$

In this thesis standard regularizer as given in equation (3.6) as well as all the four DA models as mentioned in Equation (3.10) - (3.13) have been used separately and compared their output as fraction images. The qualitative shapes of these models have been shown in figure (3.3), these figures helps to visualize how the DA models perform smoothing.

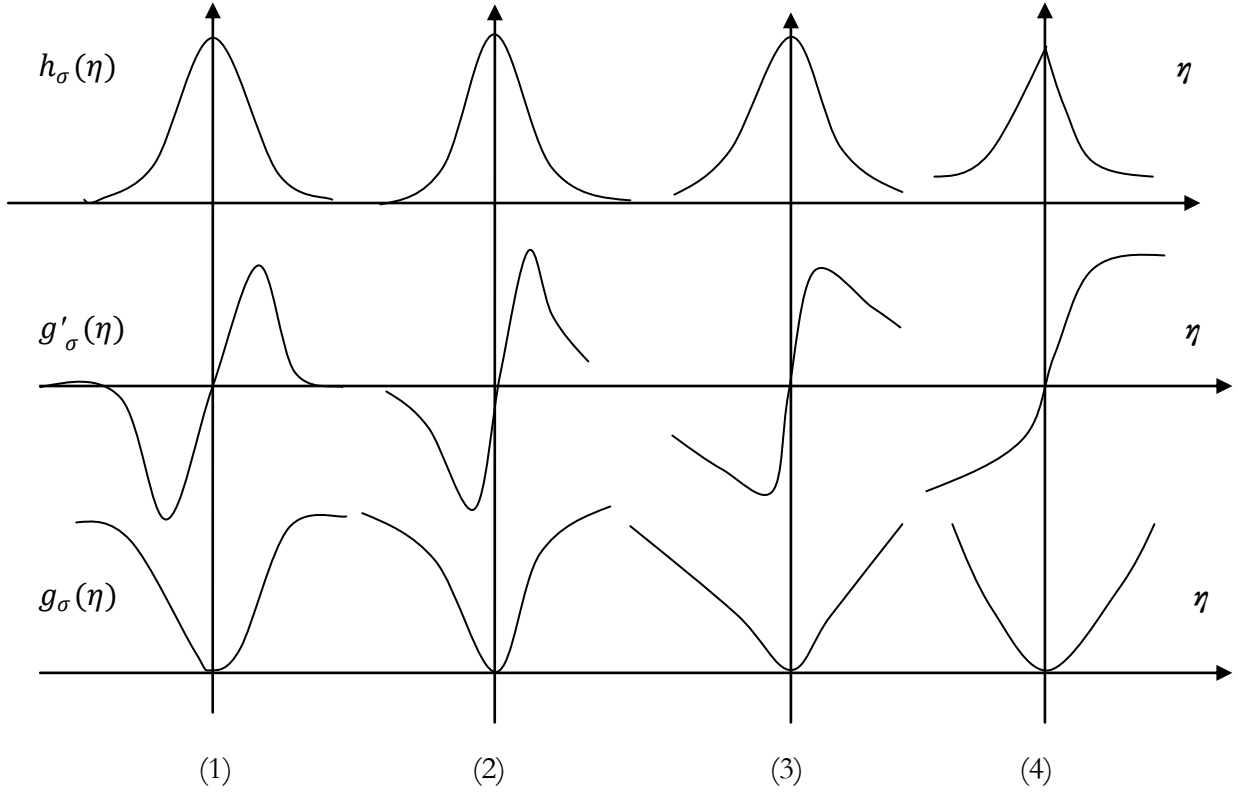


Figure 3.3: Qualitative shape of four DA functions [7]

3.8. Maximum A Posterior Solution (MAP)

MAP solution can be obtained by minimizing the global posterior energy. The combination of prior energy and conditional energy is the posterior energy solution. According to the Bayesian formula, the MAP solution can be obtained as given in equation (3.14) [40].

$$P(\mu|d) = \frac{P(d|\mu)P(\mu)}{P(d)} \quad \text{Equation (3.14)}$$

where μ is the membership value and d is the given dataset. Minimization of the posterior probability can be done as shown in equation (3.15).

$$\mu = \arg \max\{p(\mu|d)\} \quad \text{Equation (3.15)}$$

From equation (3.4) the MAP estimate is equivalent to the minimization of global energy function and can be expressed as given in equation (3.16).

$$\hat{\mu} = \arg \min\{U(\mu|d) + U(\mu)\} \quad \text{Equation (3.16)}$$

where, $\hat{\mu}$ is the optimal membership value of a class after minimizing the global energy function, $U(\mu|d)$ is the conditional energy and $U(\mu)$ is the prior energy function. The global posterior energy function can be defined as given in equation (3.17).

$$U(\mu|d) = U(d|\mu) + U(\mu) \quad \text{Equation (3.17)}$$

To control the balance between this two energy function one additional parameter λ termed as smoothness strength is added. The value of λ varies between 0 and 1. The re-written function is given in equation (3.18).

$$U(\mu|d) = (1 - \lambda)U(d|\mu) + \lambda U(\mu) \quad \text{Equation (3.18)}$$

Minimization of the global posterior energy function is needed to obtain the MRF-MAP estimate. Simulated annealing (SA) algorithm has been used to find out the global minimal energy and it has been proven that SA performs better than the other existing method [6].

3.9. Formulation of FCM Objective function to incorporate contextual information

To solve a problem using MAP-MRF it is important first to formulate the objective function. Here, the objective function of FCM has been formulated for the smoothness prior and for discontinuity adaptive priors that are able to incorporate contextual information. The objective function is similar to the objective function of FCM except for the inclusion of neighbourhood information. The objective function of FCM is given in equation (3.19), more details on FCM have been explained in appendix A.

$$J_m(U, V) = \sum_{j=1}^N \sum_{i=1}^c \mu_{ij}^m |X_j - V_i|^2, \quad 1 \leq m < \infty \quad \text{Equation (3.19)}$$

The objective function in (3.19) calculates the membership values for pixels based on spectral properties, but it does not include spatial contextual information. In equation (3.20)-(3.24), objective functions have been formulated that incorporate spatial contextual information using either the smoothness prior or discontinuity adaptive priors.

Equation (3.20) states the FCM objective function formulated using smoothness prior. From now onwards the objective function in equation (3.20) will be referred as FCM-S.

$$U(\mu_{ij}|d) = (1 - \lambda) \left[\sum_{i=1}^N \sum_{j=1}^c \mu_{ij}^m d_{ij}^2 \right] + \lambda \left[\sum_{i=1}^N \sum_{j=1}^c \sum_{j' \in N_i} \beta \left(\mu_{ij} - \mu_{ij'} \right)^2 \right] \quad \text{Equation (3.20)}$$

where,

$U(\mu_{ij}|d)$ = Posterior energy of image μ , given image d .

λ = Weight for spectral and contextual information (smoothness strength).

μ_{ij} = Membership value of pixel i of class j .

N = Number of pixels.

C = Number of classes.

m = Weighing exponent

$d^2 = |d_i - c_j|^2$; d_j = vector pixel value, c_j = mean vector of class j .

β = Weight for neighbors.

N_i = Neighborhood window around pixel i .

In Equation (3.20) spectral information has been included by using the objective function of FCM and spatial contextual information was incorporated by using smoothness prior. FCM objective functions formulated with discontinuity adaptive priors (DA prior) are given in equations (3.10) - (3.13). As discussed in section 3.7, all the four DA priors have been used to formulate the FCM objective function to incorporate spatial contextual information while avoiding over smoothing at the edges. Let η , be defined as $\mu_{ij} - \mu_{ij'}$ i.e. the difference between target pixels (pixel i) membership value and the membership of its neighboring pixels membership value in a neighborhood system N_i . Then

$$U(\mu_{ij}|d) = (1-\lambda) \left[\sum_{i=1}^N \sum_{j=1}^C \mu_{ij}^m d_{ij}^2 \right] + \lambda \left[\sum_{i=1}^N \sum_{j=1}^C \sum_{j' \in N_i} \left(-\gamma e^{-\frac{\eta^2}{\gamma}} \right) \right] \quad \text{Equation (3.21)}$$

$$U(\mu_{ij}|d) = (1-\lambda) \left[\sum_{i=1}^N \sum_{j=1}^C \mu_{ij}^m d_{ij}^2 \right] + \lambda \left[\sum_{i=1}^N \sum_{j=1}^C \sum_{j' \in N_i} \left(-\frac{\gamma}{1 + \frac{\eta^2}{\gamma}} \right) \right] \quad \text{Equation (3.22)}$$

$$U(\mu_{ij}|d) = (1-\lambda) \left[\sum_{i=1}^N \sum_{j=1}^C \mu_{ij}^m d_{ij}^2 \right] + \lambda \left[\sum_{i=1}^N \sum_{j=1}^C \sum_{j' \in N_i} \left(\gamma \ln(1 + \frac{\eta^2}{\gamma}) \right) \right] \quad \text{Equation (3.23)}$$

$$U(\mu_{ij}|d) = (1-\lambda) \left[\sum_{i=1}^N \sum_{j=1}^C \mu_{ij}^m d_{ij}^2 \right] + \lambda \left[\sum_{i=1}^N \sum_{j=1}^C \sum_{j' \in N_i} \left(\gamma |\eta| - \gamma^2 \ln(1 + \frac{|\eta|}{\gamma}) \right) \right] \quad \text{Equation (3.24)}$$

where, all the symbols have common meaning. In addition, γ is the AIF as explained in section 3.7, with a value varying between 0 and 1. As explained in section 3.7, adaptive potential

functions (APF) have been used in equations (3.21) - (3.24) to formulate the objective function of FCM with discontinuity adaptive priors. From now onwards, the objective functions mentioned in (3.21)-(3.24) will be referred as FCM DA-MRF (H1), FCM DA-MRF (H2), FCM DA-MRF (H3) and FCM DA-MRF (H4) respectively.

3.10. Simulated Annealing and Gibbs sampling algorithm

Simulated annealing (SA) was first introduced by Metropolis *et.al* [42] to simulate particle behavior in a thermal equilibrium. SA is a stochastic relaxation algorithm to determine the global minimum solution. The idea of SA is similar to a process of metallurgy where the metal is heated up to a certain limit to reconstruct it in a desired shape. Then the metal is cooled down very slowly so that it gets enough time to respond. The SA algorithm is frequently used in MRF model based image analysis to find the global optimum solutions [3], [4], [5]. Here SA is used to find optimum global energy function.

The SA algorithm designed by Geman and Geman [3] is known as the Gibbs sampler. It generates new membership values for each pixel. In order to do so, it depends upon a parameter T , called the temperature. SA starts with a high value of T and then the value of T is decreased according to specific criteria, called the cooling schedule. The process runs till the value of T reaches zero. In this work the cooling schedule given by Dubes and Jain has been used as mentioned in Equation (3.25).

$$T_{k+1} = \frac{\ln(1+k)}{\ln(2+k)} T_k \quad \text{Equation (3.25)}$$

The temperature cooling function mentioned in equation (3.25) has been used here because it decreases the temperature T faster than other existing methods [6].

3.11. Parameters to be estimated

The objective functions mentioned in equations (3.20) and (3.21) - (3.24) involves the parameters as listed in (a)-(e). It is necessary to estimate the parameters before the objective functions can be used for classification [5]. The following parameters have been optimized.

- (a) Fuzzifier (m)
- (b) Initial (T_0) and final temperature(T_f)
- (c) Lambda (λ)
- (d) Beta (β)
- (e) Gamma (γ)

There have been no standard methods to estimate the parameter. Several method such as RMSE, total energy etc. have been used in the past to estimate these parameters [40],[43]. In this work, estimation of parameter has been conducted using the entropy method [33]. The entropy method gives an absolute measure of uncertainty and at the same time edge preservation was also checked by mean and variance method to estimate the parameters. The Entropy method was discussed in section 3.13.3 and the mean and variance method for edge preservation was explained in detail in section 3.12.

3.12. Mean and variance method to verify edge preservation

A main aim of this work was to develop a discontinuity adaptive MRF model based contextual classifier. Therefore, it is important to verify that the edges for classified output were correct. An edge represents the boundaries between two objects. An edge can be characterized as a step function or slop between two regions [44]. As per Wen and Xia [44] , if for some specific threshold c , $|\mu_1 - \mu_2| \leq c$, then there is no significant difference between the grey levels on the two sides of the edge whereas if $|\mu_1 - \mu_2| > c$ then there is significant difference between the true averages. Where μ_1 and μ_2 are the mean value of the pixels grey level on the each sides of the edges. To verify whether or not an edge is significant, an ideal way is to analyze separately the distributions of grey levels of the two regions on either side of the edge, where the difference between the average values within the two regions indicates the steepness of the edge [44]. To determine the value of c , edge point is examined first. An edge point is retained if;

$$|X_i - Y_i| > c + \sqrt{2}SZ_\alpha \quad \text{Equation (3.26)}$$

where, X_i and Y_i represents the grey level of i th pixel on the two sides of the edge respectively. S is the standard deviation of the grey levels in the region the point belongs to. Z_α can be obtained from the standard distribution tables. In practice $\alpha = 0.01, 0.05, 0.1, 0.2$ etc. is taken depending on different requirement. Both the low and high thresholds for edge can be identified by selecting two different α values.

In this work the developed contextual classifier generates a fraction image for every class. The membership value of a unit in a fraction is high if the pixel exists at a location of a known class and for the unknown class it is low. In the fraction image, among the membership values variability will be less if the area is homogeneous. Consequently, the mean of the membership value will be high and the variance will be low in case of a homogeneous area for a known class location in a fraction image. This concept has been used here to verify the edge preservation. In [41] a similar concept has been used to verify edge for the classified output of fraction image.

In the current method as shown in figure (3.4) a homogeneous area of a specific class i.e. crop has been selected which has a high mean value and a low variance. After selecting a homogeneous area, two sets of pixels were selected at either side of the edge. Mean and variance were calculated for these two set of pixels at each lambda varying between 0 and 1. The mean difference of these two set of pixels should be high and variance would be low if the edge is preserved (Figure 3.4).

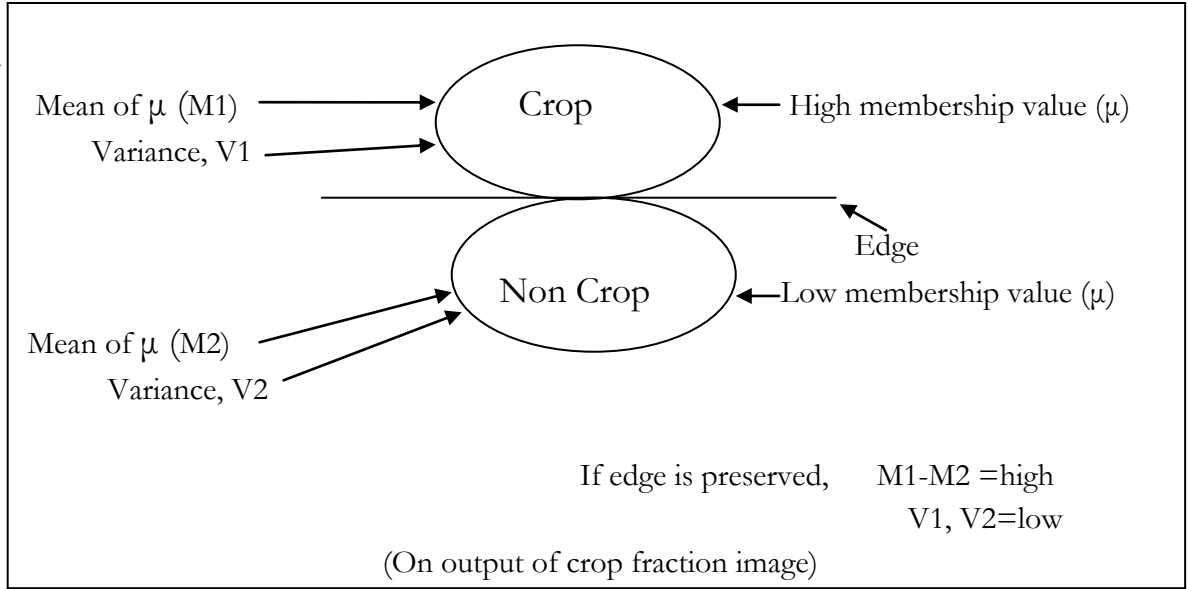


Figure 3.4: Method to verify edge preservation

3.13. Methods adopted for accuracy assessment

Accuracy assessment of classified output is necessary to obtain the quality of the results. In this work where an image to image based accuracy assessment technique has been used, the accuracy of the classification of a coarser resolution images was evaluated with the classified output of a finer resolution image. In this section, accuracy assessment techniques for the sub-pixel classified outputs that have been used for this research work have been described.

3.13.1 Fuzzy Error Matrix

To assess the accuracy of a classified output, the testing samples from classified fraction output and the reference data from actual class were collected. Using these test samples a fuzzy error matrix was generated using the specific operator as in equation (5.9). The columns represent the actual classes from the reference data, while rows represent the classes of the classified data. In this matrix the diagonal elements indicate the classes which are correctly classified and the off-diagonal elements indicate the misclassified classes. Fuzzy Error Matrix (FERM) [9] is similar to a conventional error matrix. The conventional error matrix takes hard classified images as input whereas FERM takes fraction images as its input. In FERM the elements of the matrix are calculated based on the fuzzy set theory [1]. It uses the 'MIN' operator (3.27), which identifies the maximum possible overlap between reference and classified datasets. The MIN operator is known as fuzzy set intersection operator [31].

$$\min(S_{nk}, r_{nl}) \quad \text{Equation (3.27)}$$

where, S_{nk} is the membership grade of class k at pixel n for the assessed dataset.
 r_{nl} is the membership grade of class k at pixel n for the reference dataset.

3.13.2 Sub-pixel confusion uncertainty matrix

A new cross comparison matrix was proposed by Silvan-Cardenas and Wang [31] that used confusion interval in the form of plus-minus maximum error to measure the sub-pixel accuracy. This new error matrix is referred to as sub-pixel confusion uncertainty matrix (SCM). It uses composite operator namely 'MIN-LEAST', 'MIN-MIN' and 'MIN-PROD'. These operators have been described below.

- The MIN-MIN composite operator is formed by one single operator i.e. MIN operator. For both diagonal and off-diagonal elements this composite operator uses the minimum operator. This operator assigns diagonal elements in a first step and then it calculates the off-diagonal elements based on the over and underestimation errors [31].
- The MIN-LEAST composite operator is formed by the two basic operators MIN and LEAST. Here the MIN operator is for the diagonal cells and the LEAST operator is for the off-diagonal cells. The MIN operator measures the maximum sub-pixel overlap among the classes and the LEAST operator measures the minimum possible sub-pixel overlap between two classes [31]. This MIN-LEAST operator creates a diagonal matrix for a perfect matching case [31].
- The MIN-PROD composite operator was proposed by Pontius and Cheuk [32]. It uses the MIN operator for the diagonal cells and PROD operator for the off-diagonal cells. The diagonal cells give the maximum overlap between the reference and assessed classes. The off-diagonal cells measure the expected overlap of reference and assessed classes.

3.13.3 Entropy method

Classification accuracy is generally measured by an error matrix, but for this work generation of reference data for LISS-IV image was not possible because of the unavailability of further higher resolution image for the study area as well as it is not possible to generate fraction reference output from ground with large number of samples. In such case entropy [33] is used as an absolute measure of uncertainty. Entropy calculates the uncertainty from the classified data without using any external data so it is an indirect method to measure accuracy. The entropy of a classified fraction output can be calculated by equation (3.28). For a better classified output the entropy at known class will be low and at unknown class it will be high in a fraction image of a class. For example if in fraction image of crop, the entropy value at crop location will be low whereas entropy value other than crop location will be high. Thus low uncertainty implies more accurate classified output and vice-versa. The mathematical formula for entropy is given in equation (3.28).

$$Entropy(x) = \sum_{i=1}^C -\mu(w_i/x) \log_2(\mu(w_i/x)) \quad \text{Equation (3.28)}$$

where, c is the total number of classes and $\mu(w_i/x)$ is the estimated membership function of class i for pixel x .

For high uncertainty, the value of entropy in equation (3.28) is high and inverse. Entropy is defined based on actual output of classifier so it can give the pure uncertainty of the classification results [33]. In this research work entropy has been used combining with edge preservation measure to optimize the parameters of MRF model.

4. Study area and Data used

This chapter describes the study area, the data used and their pre-processing. It also includes the generation of reference data set.

4.1. Study area

The study area selected for this research work was Sitarganj Tehsil which is located near the Pant Nagar under Uttarakhand state, India. Sitarganj's geographic lat/long extends from 28°53'57.12''N to 28°56'31.22''N latitudes and 79°34'22.92''E to 79°36'35.27''E longitudes. The 'G.B Pant University of Agriculture and Technology' is located in Pant Nagar which participated during green revolution of India. This is the first Agricultural University of India since 1960 and Pant Nagar is famous for this. For this research work Sitarganj has been selected as a study area because field work data as well as satellite images of Resourcesat-1 acquired on October 2007 was available. Also the images of Resourcesat-2 were acquired for the study area. The study area presents different land cover classes like Sal forest, eucalyptus plantation, agricultural land with sugarcane and paddy as major crops and two water reservoirs namely, Baigul reservoir and Dhora reservoir (Figure 4.1). The study area presents two types of edges or boundaries among the land cover classes. (a) The sharp distinct edges among the agricultures fields and (b) The boundaries which changes gradually from one class to another such as in water class water changes gradually to grass land.

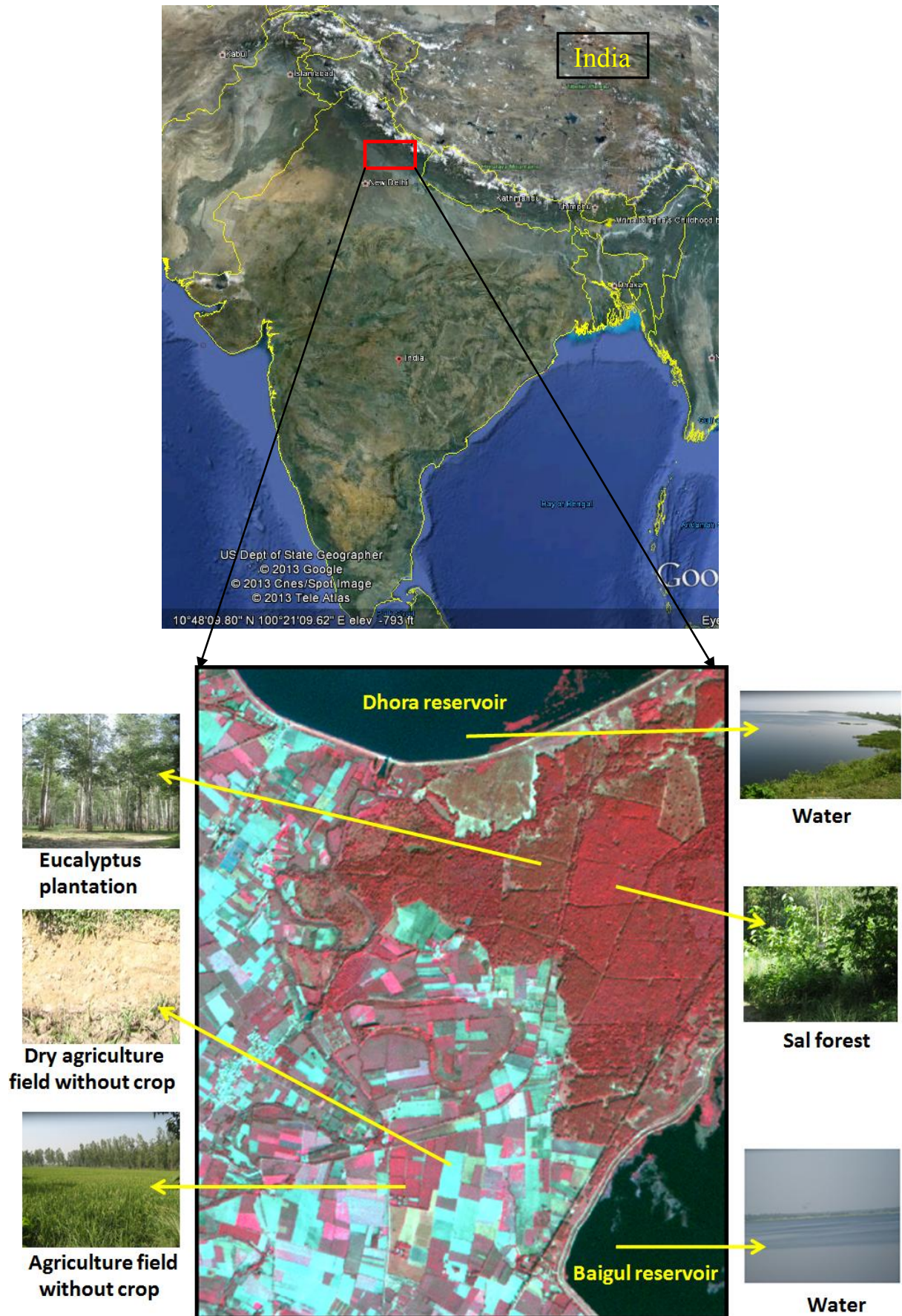


Figure 4.1: Location of Sitarganj study area (*source*: Google Earth, accessed on 11th Jan 2013)/ LISS-IV (Resourcesat-2)/ Field photographs

4.2. Data used

In this research work, AWiFS (Advanced Wide Field Sensor), LISS-III (Linear Imaging Self Scanner) and LISS-IV images from the Resourcesat-1 (Indian Remote sensing Satellite-P6) and the Resourcesat-2 (Indian Remote sensing Satellite-P6) satellites have been used (table 4.1). The images were acquired on the same date for all the sensors from each individual satellite. LISS-III and AWiFS images have been used for classification, whereas the finer resolution LISS-IV image has been used for the generation of reference data. Resourcesat-2 has an improved radiometric accuracy as compared to Resourcesat-1 and the developed classifier was tested on both datasets. Details of the sensors are provided in table 4.2.

Table 4.1: Images used for this research work

Satellite	Sensors	Acquiring Date
Resourcesat-1 (IRS P-6)	LISS-IV	15th October 2007
	LISS-III	
	AWiFS	
Resourcesat-2 (IRS P-6)	LISS-IV	23rd November 2011
	LISS-III	
	AWiFS	

The IRS-P6 (Resourcesat-1) satellite was launched by ISRO in October 2003. It is the 10th mission of Indian Remote Sensing (IRS) satellite series. The on-board sensors on this satellite are LISS-IV (Linear Imaging Self Scanner), LISS-III and AWiFS. Table (4.2) describes these sensors characteristics in details.

Table 4.2: Sensors specification of Resourcesat-1(R1) and Resourcesat-2(R2) (*source*: www.isro.org, accessed on 8th Jan 2013)

Specifications	LISS-IV		LISS-III		AWiFS	
	R1	R2	R1	R2	R1	R2
Spatial resolution (m)	5.8	5.8	23.5	23.5	56	56
Swath (KM)	23.9(MX Mode) 70.3(PAN Mode)	70.0 in MX mode and mono mode	141	141	740	740
Spectral Bands (microns)	0.52-0.59	0.52-0.59	0.52-0.59	0.52-0.59	0.52-0.59	0.52-0.59
	0.62-0.68	0.62-0.68	0.62-0.68	0.62-0.68	0.62-0.68	0.62-0.68
	0.77-0.86	0.77-0.86	0.77-0.86	0.77-0.86	0.77-0.86	0.77-0.86
			1.55-1.70	1.55-1.70	1.55-1.70	1.55-1.70
Quantisation (bits)	7	10	7	10	10	12

IRS-P6 (Resourcesat-2) is the follow up mission of Resourcesat-1. In April, 2011 Resourcesat-2 was launched by ISRO. The on-board sensors are LISS-IV, LISS-III and AWiFS. The major changes in Resourcesat-2 as compared to Resourcesat-1 are: improved radiometric accuracy from 7 bits to 10 bits for LISS-III and LISS-IV and 10 bits to 12 bits for AWiFS [45]. Details of the sensors for this satellite are given in Table (4.2).

4.3. Pre-processing of the data

Prior to any application it is important to perform geometric correction for all the images. Coarser resolution images should be co-registered with the fine resolution images. In this research work, an image to image accuracy assessment method was performed. Also for accuracy assessment purposes it is important to co-register the images to compare the coarse spatial resolution images with the fine spatial resolution images.

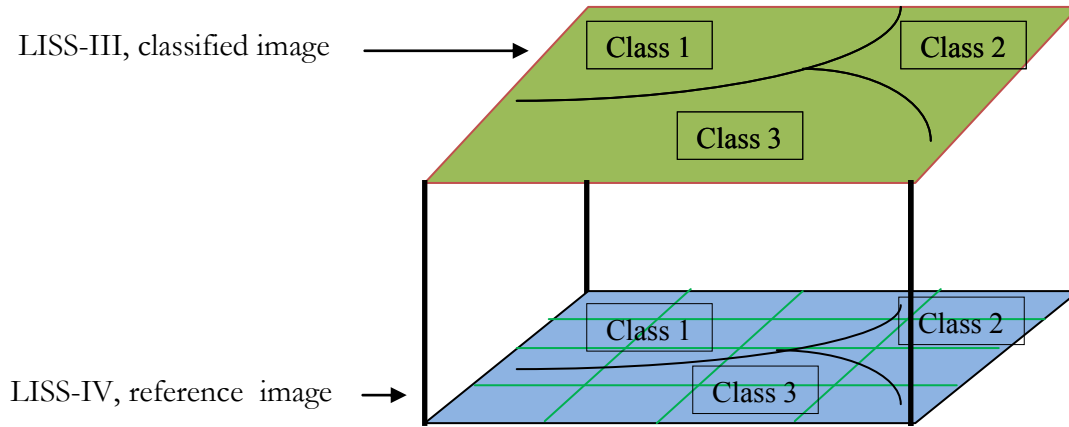


Figure 4.2: Comparing finer resolution image with coarser resolution image

For geometric correction of the LISS-IV image, the toposheet, numbered $53\frac{P}{9}$ from the Survey of India (SOI) has been used. The LISS-IV image was geo-registered in UTM projection with WGS84 North spheroid and datum, zone 44. By using nearest neighbor resample method the LISS-IV image was resampled at a 5m spatial resolution. Resampling is important for an accuracy assessment as finer resolution image has been used as a reference image for classified coarser resolution images. Resampling is required for geometric transformation, and it is like convolving the input image with a uniform weighing function. All the three images (LISS-IV, LISS-III and AWiFS) were resampled at 5m, 20m, and 60m spatial resolution to form a ratio of 1:4:12, respectively. In doing so correspondence between LISS-III and AWiFS pixels were maintained with particular number of LISS-IV pixels i.e. 16 and 144 pixels respectively for the convenience of accuracy assessment. For example as shown in figure 4.2, for a single pixel of LISS-III, 16 pixels of LISS-IV were sampled. To generate the fuzzy error matrix, for each sample the single membership value from LISS-III and the mean of 16 membership value from LISS-IV has been used.

Geo-registration of LISS-III image was done with respect to the geometrically corrected LISS-IV image taking similar projection, spheroid and datum as that of LISS-IV image. The LISS-IV image was resampled at 20 m spatial resolution.

Geo-registration of AWiFS image was done with respect to the geometrically corrected LISS-III image. The projection, spheroid and datum were same as that of LISS-III and LISS-IV images. The resampling of AWiFS image was done at 60 m spatial resolution.

4.4. Generation of reference dataset

In this research work, the LISS-IV images were used as reference data for AWiFS and LISS-III images. The reference dataset has been generated from finer resolution image instead of using field data because of the following listed reasons.

- (a) It is difficult to locate within pixel classes on the ground exactly.
- (b) Reference data generation from field survey is a type of classification and may contain errors [12].
- (c) A field visit may not always possible due to inaccessibility of study area.
- (d) Correct identification of classes on the ground may be difficult at the sub-pixel level [12].
- (e) As the main issue is landcover, field data may not provide additional information as compared to high resolution satellite images.

To evaluate the classified dataset it is also necessary to classify the reference dataset. There are two methods available to generate soft reference data set from finer resolution image.

Method 1: Classify the LISS-IV image by traditional hard classifier and aggregate the output to get coarser resolution soft output of LISS-III and AWiFS.

- *Advantage of the method:* From original fine resolution dataset the accuracy can be assessed of hard reference data. Hard classified LISS-IV image can be compared with the original LISS-IV to generate error matrix and assess the accuracy of the reference data.
- *Disadvantage of the method:* For fine resolution LISS-IV image it is assumed that the pixels are pure but it is not always true. LISS-IV image with 5m resolution may contain mix pixels.

Second disadvantage of this method is that the soft output for coarser resolution images were generated by aggregating hard classified output. So the partial membership is due to the proportion of the pixel that form the class but not for the uncertainty or ambiguity in class definition. Hence the reference data generation from this method to assess the accuracy of fuzzy classified output is not suitable.

Method 2: Use sub-pixel classifier to generate soft reference data from fine resolution-IV image.

- *Advantage of the method:* In this method all the pixels of fine resolution dataset are not assumed as a pure pixel.

Second advantage of this method is that the membership values are generated due to the uncertainty or ambiguity of class definition. So the second disadvantage of method 1 can be avoided by this method.

- *Disadvantage of the method:* The resolution of classified dataset is different from reference dataset. To compare the reference dataset with the classified dataset the reference dataset is either resampled or aggregated to a mean pixel. In doing so there may occur error. If the classifier for the reference data set and classified dataset are different two cases may arise. First, the performance of the classifier used for image classification may be better

than reference classifier. Second the performance of classifier dataset is better in terms of accuracy than the reference dataset.

In this research work, the same classifier has been used for both the image classification and reference data generation. This remove the disadvantage of use the different classifiers and error occurred only due to difference in resolution of the images.

5. Results

This chapter presents the estimated parameter values and classification results obtained from different classification methods. Section 5.1 describes the results of estimated parameter. In section 5.2 classification results of FCM have been given. The classification results for coarser and medium resolution dataset for FCM-S and FCM DA-MRF classifiers have been presented in sections 5.3 and 5.4 respectively. Sections 5.5 and 5.6 present the results of untrained classes.

5.1. Estimated parameter

The parameters explained in chapter 3, of fuzzy and contextual classifiers have been estimated and given in this section.

Fuzzifier (m): Fuzzifier, m is the membership weighing exponent, $1 \leq m < \infty$ which controls the degree of fuzziness in FCM classification. As $m \rightarrow 1$ the solution of the FCM becomes crisp or hard, this means that pixel's membership value become closer to 1 or 0, while the value of m is greater (e.g., 2 or more), the membership assignment will be fuzzier, this represents that the membership value for all classes are closer to each other [6]. According to [46], [47] the value of m should be between 1.3 and 2.5. In this study the value of m is taken as 2.2.

Initial temperature (T_0): According to [3], [40], [43] initial temperature T_0 should be 3 or 4 for the most image analysis application. In [41] entropy has been used to estimate the MRF model based PCM classification parameters Thus in this research work to justify the value of T_0 entropy value of the classified output has been calculated.

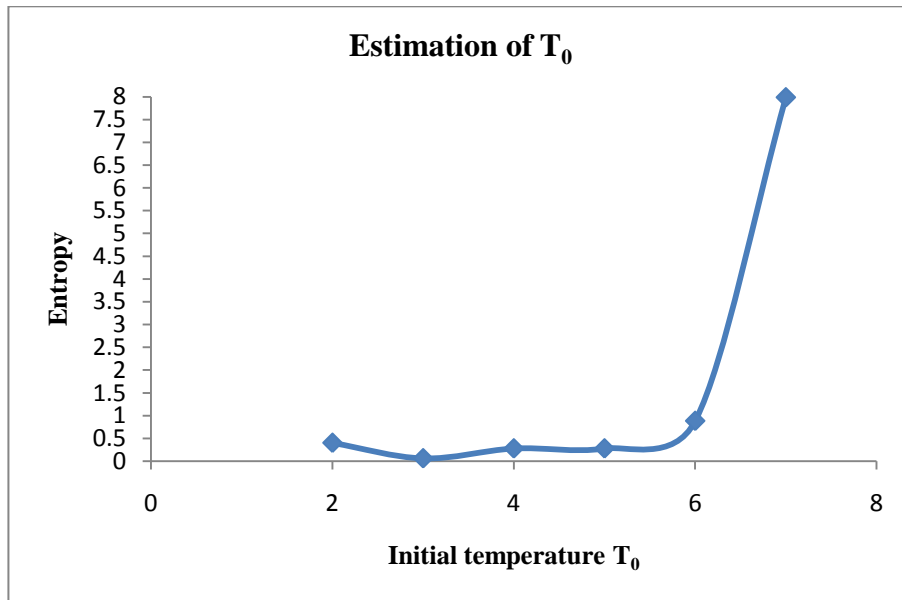


Figure 5.1: Estimation of Initial Temperature T_0

During the optimization process other parameters were kept fixed. The entropy values calculated for initial temperature $T_0 = 2, 3, 4, 5, 6, 7$ as given in figure (5.1) and it was found that the value of T_0 above 4 does not provide improvement. Hence, for this study $T_0 = 3$ has been selected for all experiments.

Lambda (λ): As mentioned in the section 3.8, chapter 3, λ is the smoothness parameter that controls the balance between spectral and spatial information. This parameter is involved in FCM-S and in FCM DA-MRF models. To optimize this parameter entropy was calculated and edge preservation was verified parallelly. It is important to verify edge preservation in this work because here the developed contextual classifier is for discontinuity adaptive image classification. In figure (5.2) optimization of λ and β for LISS-IV for FCM-S has been provided. The value with minimum entropy has been taken as optimized parameter. The less entropy lies in the ranges of 0.6 to 0.9 and 1 to 3 for λ and β respectively; along with this edge verification was checked for each λ and β to determine the optimum value as given in table (5.1) and (5.2). For edge verification the difference of mean and variances were calculated at the either sides of the edges as discussed in section 3.4, chapter 3. In table (5.4) optimized parameter values for all the models were given for LISS-IV, LISS-III and AWiFS dataset.

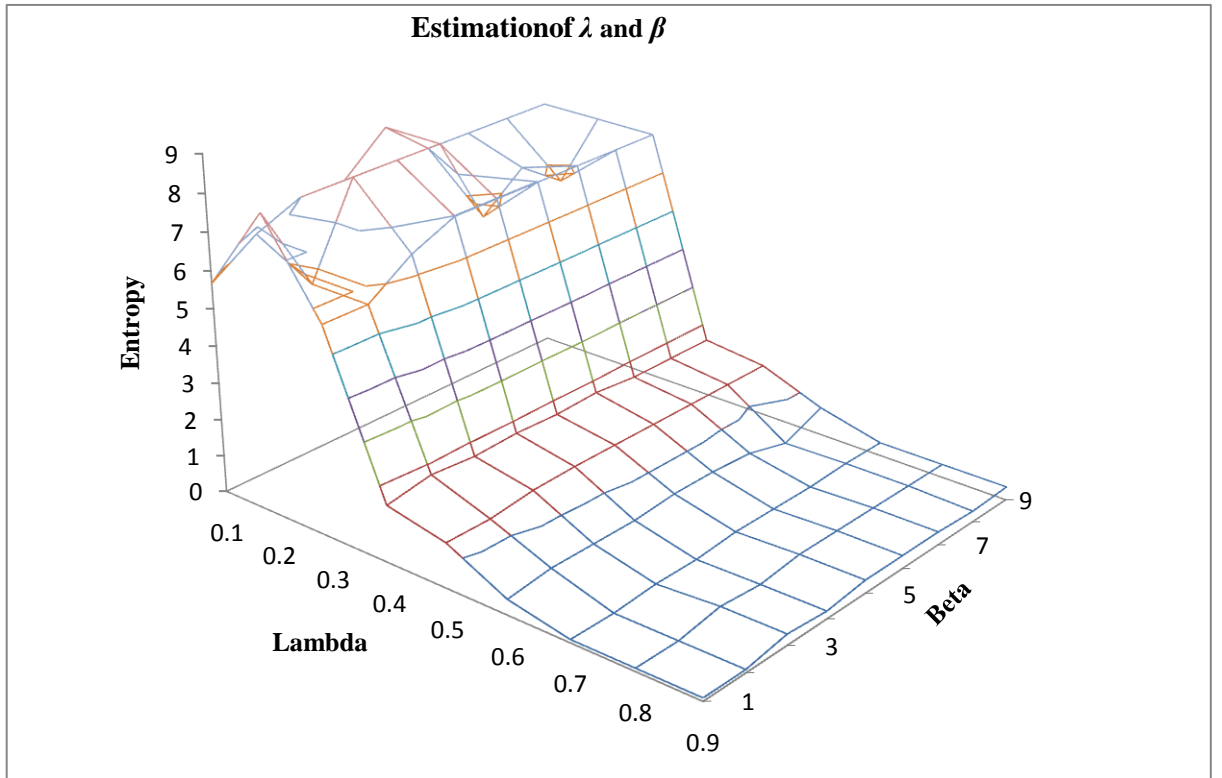


Figure 5.2: Estimation of λ and β

Table 5.1: Verification of edge preservation for λ values

Lambda Values (λ)	Difference in mean	Variance
0.2	1.33	0.166, 0.566
0.3	176.66	7822.167, 6.966
0.4	209.666	66.166, 7.666
0.5	208.5	66.166, 3.866
0.6	208.5	66.166, 3.866
0.7	208.666	66.166, 3.366
0.8	208.666	66.166, 3.366
0.9	208.5	66.166, 3.866

Table 5.2: Verification of edge preservation for β values

Beta Values (β)	Difference in mean	Variance
1	-0.2	0.3, 0.2
2	245.4	27.5, 1.8
3	243.8	27.5, 2.2
4	243.8	27.5, 2.2
5	243.8	27.5, 2.2
6	244.2	27.5, 3.2
7	243.8	27.5, 2.2

Table 5.3: Verification of edge preservation for γ values

Gamma Values (γ)	Difference in mean	Variance
0.1	246.4	37.5, 3.8
0.2	247.2	37.5, 0.2
0.3	247.2	37.5, 0.2
0.4	247.2	37.5, 0.2
0.5	247.2	37.5, 0.2
0.6	247.2	37.5, 0.2
0.7	247.2	37.5, 0.2
0.8	247.2	37.5, 0.2
0.9	247.2	37.5, 0.2

In table (5.1), (5.2) and (5.3), verification of edge preservation has been presented respectively for λ , β and γ . It has been observed from the table (5.1)-(5.3) that at $\lambda = 0.7$, $\beta = 2$ and $\gamma = 0.2$ the edge is preserved with high mean difference and low variance.

Table 5.4: Optimized parameter value

Classifiers and parameters	AWiFS	LISS-III	LISS-IV
FCM-S (λ/ β)	0.9/2	0.9/2	0.7/ 2
FCM DA-MRF (H1) (λ/ γ)	0.7/0.2	0.7/0.2	0.7/0.2
FCM DA-MRF (H2) (λ/ γ)	0.9/0.4	0.9/0.4	0.9/0.3
FCM DA-MRF (H3) (λ/ γ)	0.9/0.2	0.9/0.2	0.6/0.2
FCM DA-MRF (H4) (λ/ γ)	0.9/0.5	0.9/0.5	0.8/0.4

In this study as mentioned in section 4.2, chapter 4, two datasets from Resourcesat-1 and Resourcesat-2 has been used. For both the dataset the optimized parameter values were found same.

Beta (β): β is the weight given to the neighboring pixel in a window in FCM-S model. This has been explained in chapter 3. Similarly like lambda optimization the entropy and edge preservation have been checked to determine the optimized value for β . In table (5.4) optimized value of β is given for LISS-IV, LISS-III and AWiFS images.

Gamma (γ): γ is involved in DA models as explained in chapter 3. It determines the rate at which AIF reaches zero and controls the interaction between two pixels [25]. Estimation of γ has been conducted by calculating entropy values as well as by verifying edge preservation. In table (5.4) optimized value of γ has been given for LISS-IV, LISS-III and AWiFS images.

5.2. Results of FCM Classification

Based on the visual interpretation of LISS-IV, LISS-III and AWiFS images of the Resourcesat-1 and Resourcesat-2 satellite, land cover classes selected were given in table (5.5). The image acquisition date of Resourcesat-1 was October 2007 and total six numbers of land cover classes were identified whereas image acquisition date of Resourcesat-2 was November 2011 and total five numbers of land cover classes were found. From the field data the selected classes were verified to provide appropriate land cover label. The photographs from the field visit were given in figure (5.3).

Table 5.5: Land cover classes for the study area

No of Classes	Resourcesat-1	Resourcesat-2
1	Water	Water
2	Agriculture field with crop	Agriculture field with crop
3	Dry agriculture field without crop	Dry agriculture field without crop
4	Moist agriculture field without crop	Eucalyptus plantation
5	Eucalyptus plantation	Sal forest
6	Sal forest	



Figure 5.3: Field photographs of study area

Sub-Pixel classification of study area: On observing the AWiFS and LISS-III images in figure (5.4) it has been noticed the need of sub-pixel classification for the study area. The water body present in

the bottom right corner is largely homogeneous and it changes gradually into vegetation class and this was also noticed from the field data. The agriculture fields in the study area are small, two or three pixel of AWiFS image can cover these fields as the pixel size of AWiFS is more i.e. 60 m after resampling. In case of LISS-III image dry agriculture field without crop can be distinguish from the moist agriculture without crop but in AWiFS image these classes are merged together at the boundary. As noticed in both the images the Eucalyptus plantation and Sal forest do not have a distinct boundary, this has been observed in the field visit also.

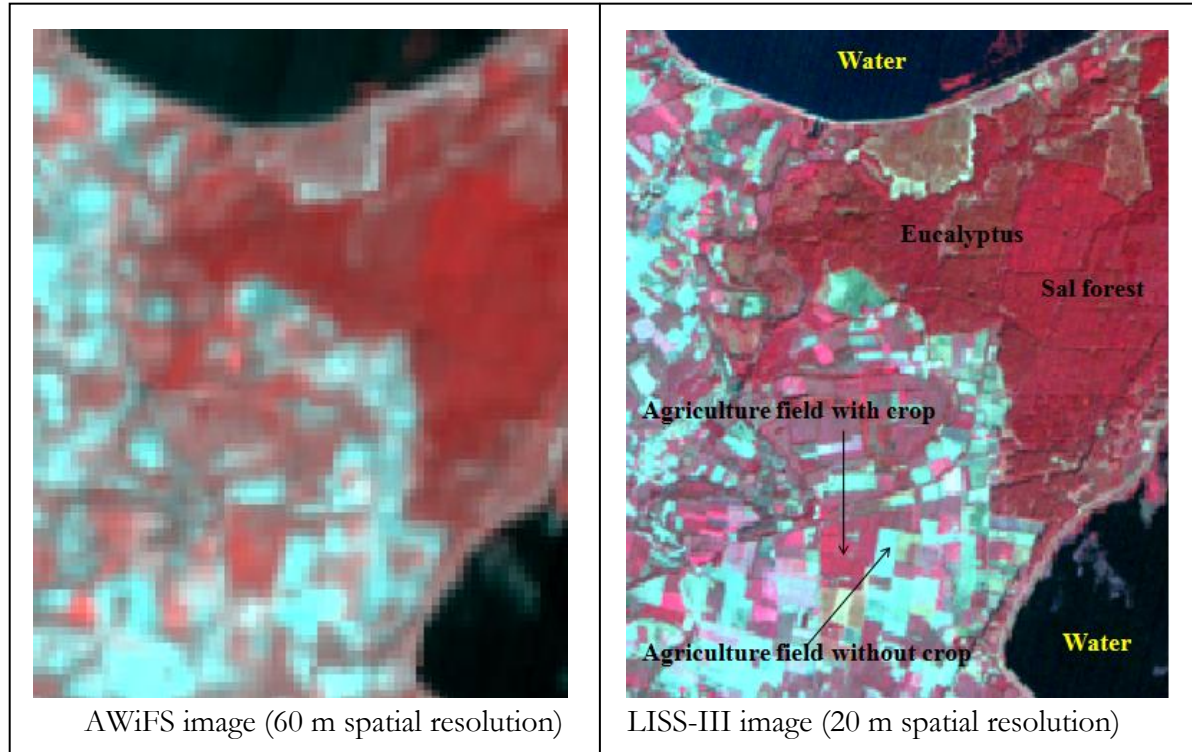


Figure 5.4: AWiFS and LISS-III images of study area

In this work accuracy assessment was conducted for all the classification results. There is no tool available commercially to assess the accuracy of the sub-pixel classified output. Thus JAVA based in house tool developed by Kumar *et al.* [48] has been used for accuracy assessment purpose. Graphical user interface (GUI) of this tool has been given in appendix B. It works based on the method of random sampling. As per the Congalton's rule [49] 75 to 100 pixels per class were considered while generating testing data.

5.2.1 FCM classification results for AWiFS images

For supervised FCM classification of AWiFS image total 50 number of training pixels were selected from each land cover classes. The training pixels were taken from well distributed area over AWiFS image. The classified fraction images of Resourcesat-1 and Resourcesat-2 were shown in figure (5.5) and (5.6).

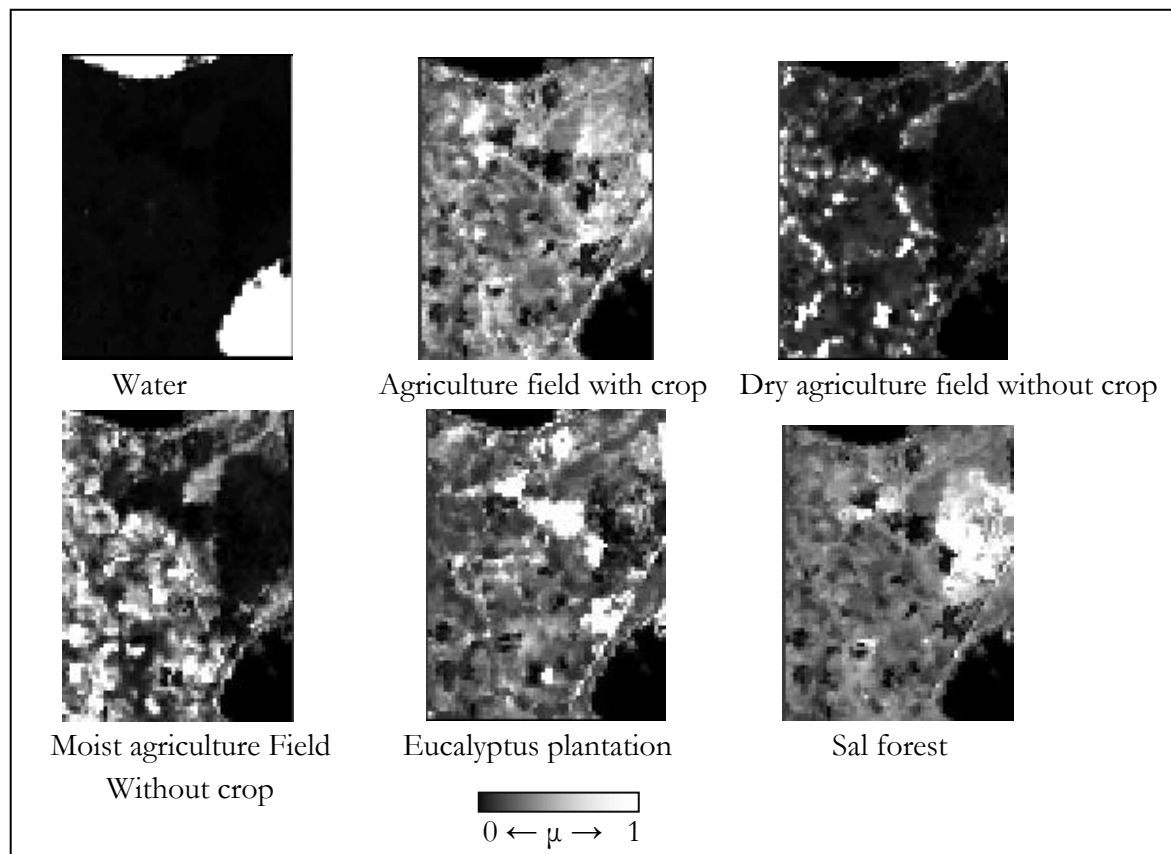


Figure 5.5: FCM classification output of AWiFS image from Resourcesat-1

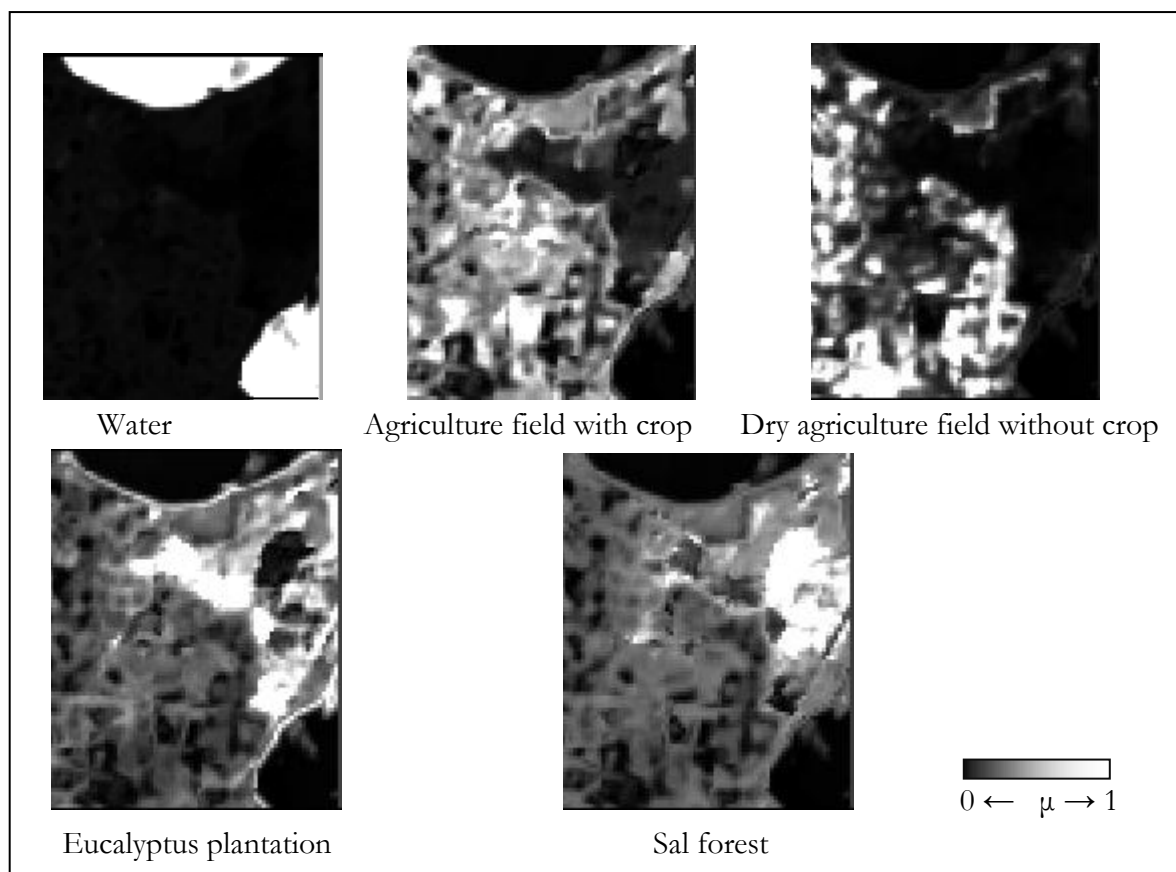


Figure 5.6: FCM classification output of AWiFS image from Resourcesat-2

From the fraction images of Resourcesat-1 and Resourcesat-2 as in figure (5.5) and (5.6), it has been observed that in Resourcesat-2, the land cover classes were well classified and more clearly visible in comparison to Resourcesat-1.

On comparing the fuzzy overall accuracy of Resourcesat-1 with Resourcesat-2 it has been found higher accuracy for Resourcesat-2 (in table C1 and C2, appendix C). As mentioned in chapter 4, the radiometric accuracy is more in Resourcesat-2 so the classification accuracy was improved for 0.94% in case of Resourcesat-2. Similarly for LISS-III images of Resourcesat-2, improved classification accuracy of 2% has been observed as compared to Resourcesat-1.

5.3. Contextual classification results for coarser resolution dataset

In this section classification result of AWiFS images from Resourcesat-1 and Resourcesat-2 for developed FCM-S and FCM DA-MRF classifiers have been presented.

5.3.1 Performance of contextual classification on AWiFS image from Resourcesat-1

This subsection presents the results of classification of AWiFS images from Resourcesat-1. The output fraction images obtained by classification using FCM-S and FCM DA-MRF has been given in figure (5.8), in FCM-S the classes were mixed with other classes as seen in class 5 i.e. Sal forest was more towards to other land cover class and the edges were also over smoothed as seen in class 6 i.e. water. But in FCM DA-MRF, classes were well classified and edges were not over smoothed. In figure (5.7) the fuzzy overall accuracy has been compared for the FCM and developed contextual classifiers considering one major fuzzy based accuracy assessment tool i.e. FERM.

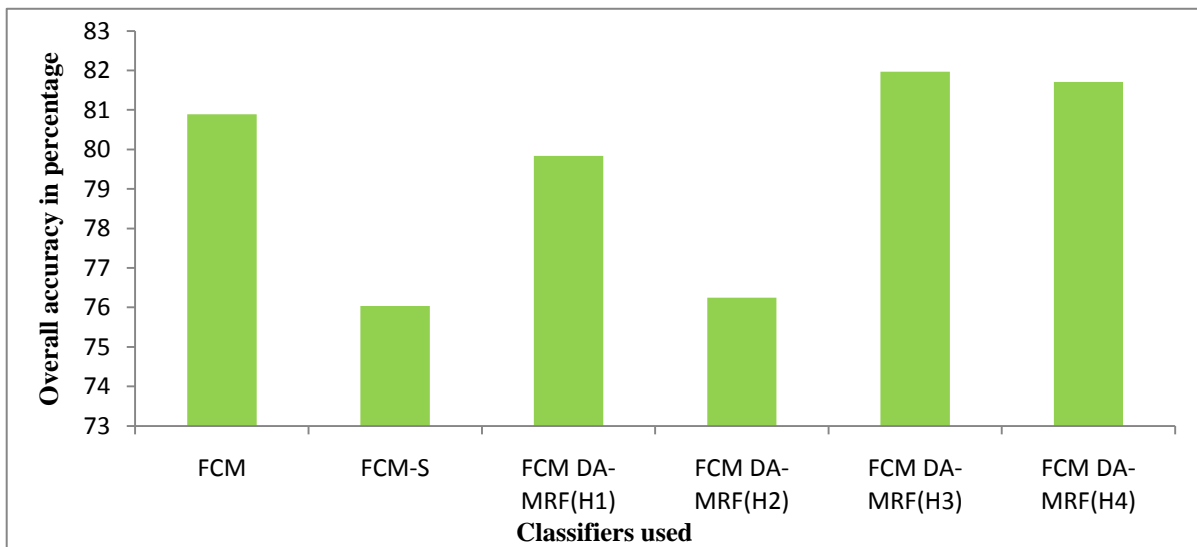


Figure 5.7: Comparison of FERM overall accuracy obtained by different classifiers for AWiFS image from Resourcesat-1

The overall classification accuracy of discontinuity adaptive contextual FCM classification was improved and it was more than 76% for all the classifiers. As compare to FCM-S the discontinuity adaptive contextual FCM classifier achieved 0.5% to 5% improvement in classification accuracy. It has been found that the FCM DA-MRF (H3) has achieved the highest overall accuracy with 81.97%. The complete fuzzy accuracy assessment reports have been provided in table (C3) - (C7) in appendix C.

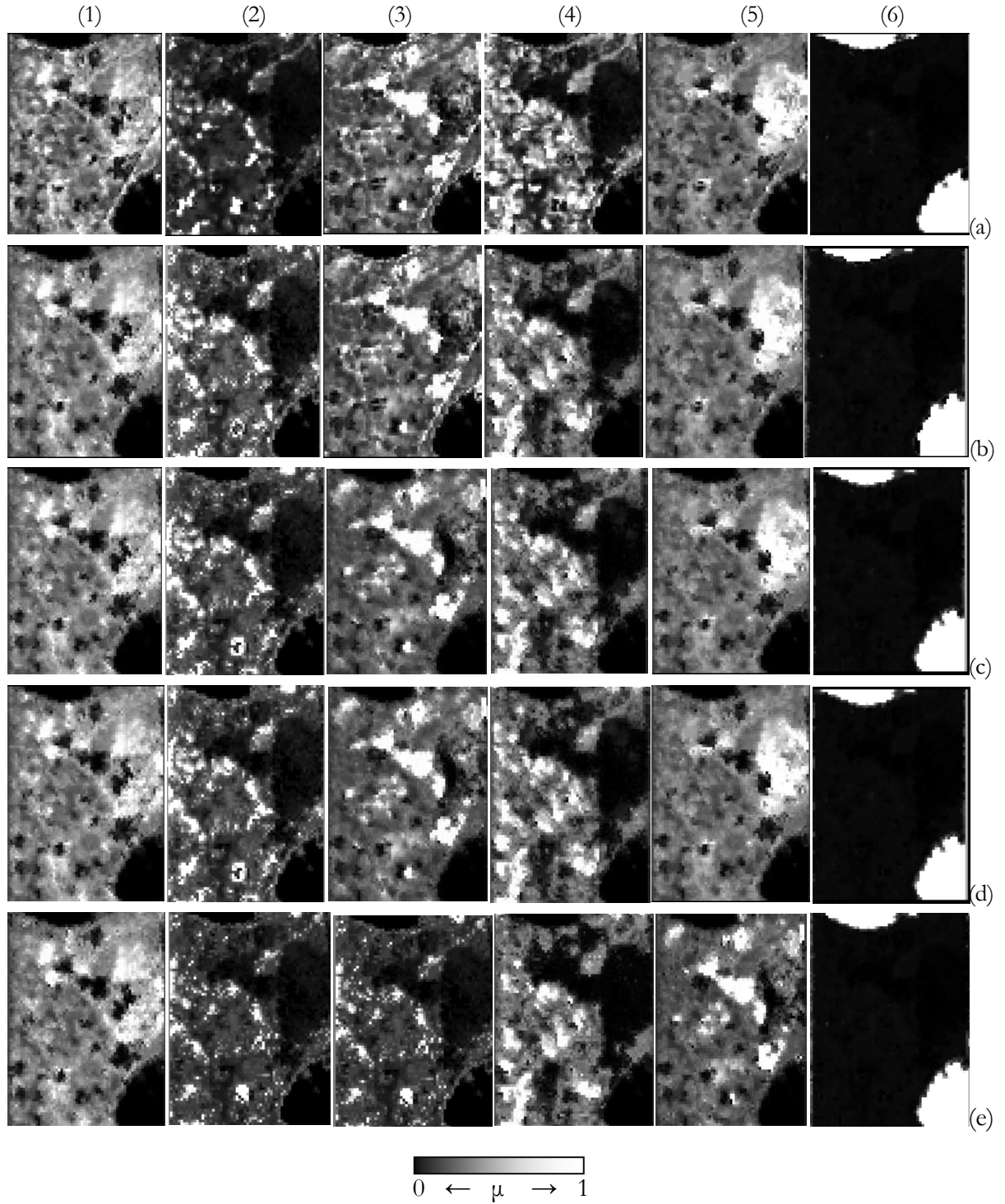


Figure 5.8: Fraction images generated from contextual FCM classification for AWiFS image from Resourcesat-1. (a) FCM-S (b) FCM DA-MRF (H1) (c) FCM DA-MRF (H2) (d) FCM DA-MRF (H3) (e) FCM DA-MRF (H4) , (1) Agriculture field with crop (2) Dry agriculture field without crop (3) Eucalyptus plantation (4) Moist agriculture field without crop (5) Sal forest (6) Water

5.3.2 Verify edge preservation

In this section edge verification has been checked for the fraction output images. Method adopted for edge verification is already explained in chapter 3. After comparing the overall accuracy for FCM-S and FCM DA-MRF it has been found that FCM DA-MRF (H3) provides best classification results with highest overall accuracy. So FCM DA-MRF (H3) has been taken as a best classifier and edge preservation was verified for this classifier output as given in table (5.6).

Table 5.6: Verify edge preservation for AWiFS from Resourcesat-1

Class	FCM-S		FCM DA-MRF (H3)	
	Difference in mean	Variance	Difference in mean	Variance
Eucalyptus plantation	153.5	1104.5, 2	157	1104.5, 0.5
Water	240	4.5, 40.5	247	4.5, 18

In table (5.6) the calculated mean and variance of the grey level for two land cover classes i.e. eucalyptus plantation and water has been presented. For a class at either side of the edges the difference in mean and variance was calculated for verification of edge preservation. Mean difference and variance is compared for FCM-S and FCM DA-MRF (H3) in table (5.6). The errors normally occurs at the edges [22], thus on preserving the edges, the overall accuracy is improved and it has been noticed in figure (5.7). Thus it is observed that the accuracy of FCM DA-MRF (H3) is higher than the FCM-S and other FCM DA-MRF models and also, it has preserved the edges.

5.3.3 Performance of contextual classification on AWiFS image from Resourcesat-2

This subsection presents the results of classification of AWiFS image from Resourcesat-2. The complete fuzzy accuracy assessment reports of AWiFS images from Resourcesat-2 have been given in table (C8) - (C12). Similarly as in figure (6.7) the classification accuracy has been compared for different classifiers for AWiFS images from Resourcesat-2 in figure (5.9).

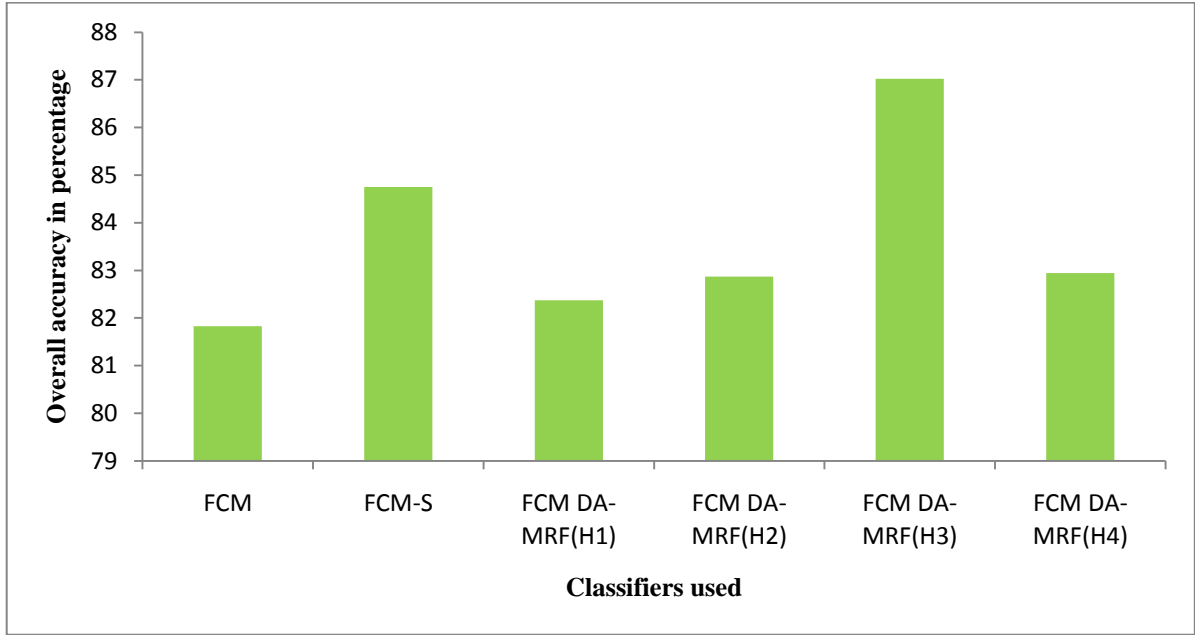


Figure 5.9: Comparison of FERM overall accuracy obtained by different classifiers for AWiFS image from Resourcesat-2

The overall classification accuracy of contextual FCM for Resourcesat-2 was improved and it was more than 82% for all the classifiers which was 1% to 8% improvement as compared to Resourcesat-1. In figure (5.9) the fuzzy overall accuracy has been compared for the developed contextual classifiers considering one major fuzzy based accuracy assessment tool i.e. FERM. Similar results like Resourcesat-1 dataset it has been found that the FCM DA-MRF (H3) can achieve the highest overall accuracy with 87.02 % whereas for Resourcesat-1 the highest overall accuracy was 81.97 %.

5.3.4 Verify edge preservation

Similarly like table (5.6), mean and variance was calculated for AWiFS fraction images from Resourcesat-2 to verify edge preservation. To verify the edges two land cover classes i.e. dry agriculture field without crop and water has been considered. The mean and variance of grey level at the two sides of the edges were calculated. The results are given in table (5.7).

Table 5.7: Verify edge preservation for AWiFS from Resourcesat-2

Class	FCM-S		FCM DA-MRF (H3)	
	Difference in mean	Variance	Difference in mean	Variance
Dry agriculture field without crop	243.8	27.5, 2.2	247.2	37.5, 0.2
Water	223.5	882, .5	244	0.5, 4.5

For both the considered classes, as stated in table (5.7), FCM DA-MRF (H3) can preserve the edges with high mean difference and low variance values in comparison to FCM-S.

5.4. Contextual classification results for medium resolution dataset

In this section classification results of LISS-III images from Resourcesat-1 and Resourcesat-2 have been presented for developed FCM-S and FCM DA-MRF classifiers.

5.4.1 Performance of contextual classification on LISS-III image from Resourcesat-1

This subsection presents the results of classification of LISS-III images from Resourcesat-1. For the LISS-III classified image fuzzy accuracy assessment was conducted and reports have been presented in table (C13) - (C17), appendix C.

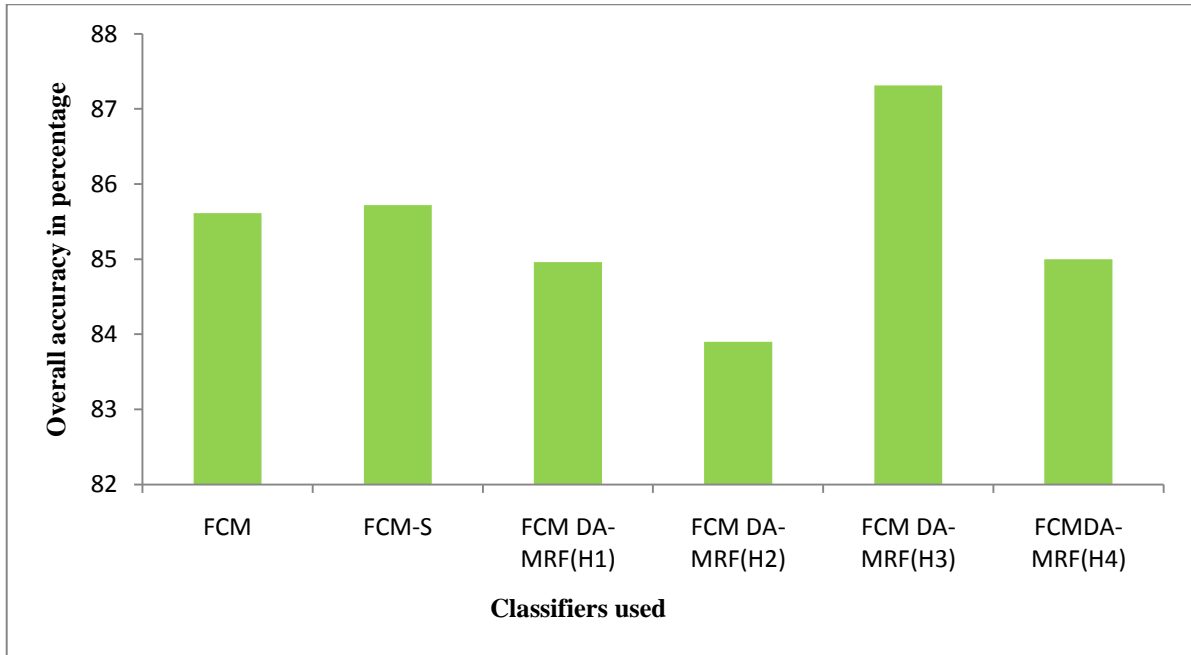


Figure 5.10: Comparison of FERM overall accuracy obtained by different classifiers for LISS-III image from Resourcesat-1

The overall classification accuracy of FCM DA-MRF (H3) was higher than other contextual model. In figure (5.10) the fuzzy overall accuracy has been compared for the developed contextual classifiers considering one major fuzzy based accuracy assessment tool i.e. FERM. It has been found that the FCM DA-MRF (H3) can achieve the highest overall accuracy with 87.31%.

5.4.2 Verify edge preservation

To verify edge preservation mean and variance was calculated for LISS-III fraction images from Resourcesat-1. Two land cover classes i.e. dry agriculture field without crop and water were considered to verify edge preservation for LISS-III image. The results were given in table (5.8).

Table 5.8: Verify edge preservation for LISS-III from Resourcesat-1

Class	FCM-S		FCM DA-MRF (H3)	
	Difference in mean	Variance	Difference in mean	Variance
Dry agriculture field without crop	216.5	4.5, 2	229.5	4.5, 2
Water	231.5	8, 4.5	239.5	2, 4.5

For both the land cover classes, FCM DA-MRF (H3) preserves the edges with high mean difference and low variance as compared to FCM-S.

5.4.3 Performance of contextual classification on LISS-III image from Resourcesat-2

This subsection presents the results of classification of LISS-III image from Resourcesat-2. Fuzzy accuracy assessment reports for FCM-S and FCM DA-MRF have been presented in table (C18) - (C22), appendix C. In figure (5.11) the fuzzy overall accuracy has been compared for the developed contextual classifiers considering one major fuzzy based accuracy assessment tool i.e. FERM.

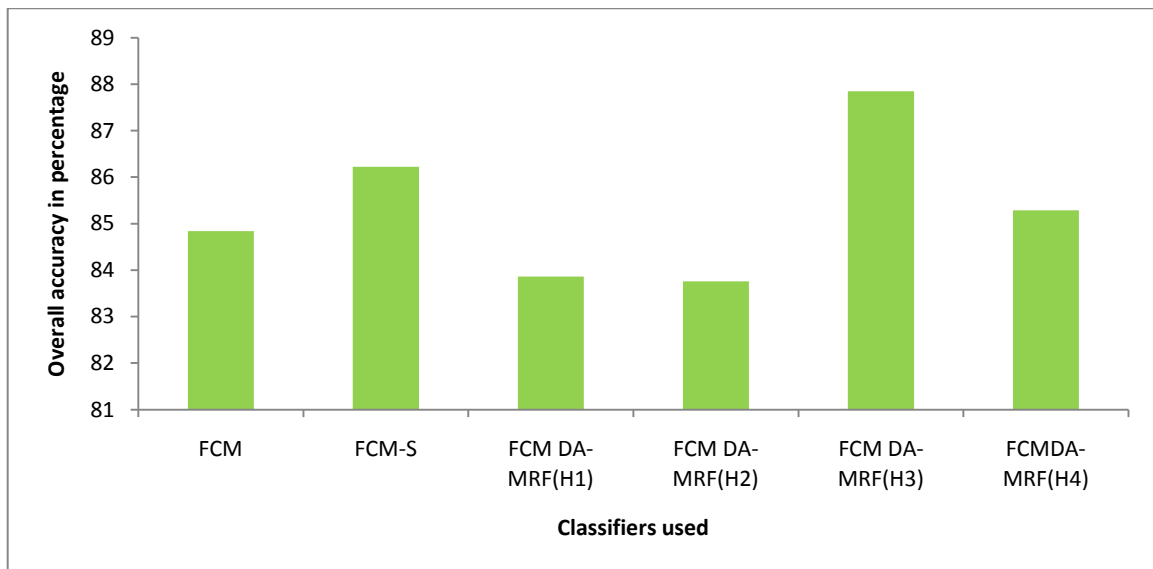


Figure 5.11: Comparison of FERM overall accuracy obtained by different classifiers for LISS-III image from Resourcesat-2

Similar like Resourcesat-1, it has been found that for LISS-III image, the FCM DA-MRF (H3) can achieve the highest overall accuracy with 87.85% for Resourcesat-2. An improvement of 1.63% has been observed in FCM DA-MRF as compared to FCM-S. The overall classification accuracy of FCM DA-MRF (H3) was higher than the other DA-MRF model also.

5.4.4 Verify edge preservation

To verify edge preservation mean and variance was calculated for LISS-III fraction images from Resourcesat-2. The results were given in table (5.9).

Table 5.9: Verify edge preservation for LISS-III from Resourcesat-2

Class	FCM-S		FCM DA-MRF (H3)	
	Difference in mean	Variance	Difference in mean	Variance
Dry agriculture field without crop	242	8, 0.5	247.5	8, 0.5
Water	224.5	264.5, 2	239	0.5, 0.5

To verify the edge preservation for LISS-III image two land cover classes i.e. dry agriculture field without crop and water has been selected and mean and variance were calculated at the two sides of the edge. The difference of the mean value was high and variance was low in FCM DA-MRF (H3) in comparison to FCM-S, it implies that FCM DA-MRF (H3) preserve the edges.

5.5. Performance of FCM-S for untrained classes

In this research work, the performance of supervised FCM-S was evaluated for untrained classes. To get the untrained class, the mean value for a known class was not provided during the training to the classifier and the classification was performed with the remaining classes [50]. Fuzzy accuracy measure FERM has been calculated to check the performance of FCM-S in case of untrained classes as given in table (5.10).

Table 5.10: Accuracy assessment report (FERM) of FCM-S classification for LISS-III image of Resourcesat-1 with LISS-IV as a reference image while class 2 (Agriculture field with crop) was not considered

Accuracy assessment method	Untrained (not considered agriculture field with crop)	Trained
Fuzzy user's accuracy (%)		
Dry agriculture field without crop	68.57	79.03
Moist agriculture field without crop	54.85	67.66
Eucalyptus plantation	69.59	84.28
Sal forest	56.28	91.47
Water	91.37	94.26
Average user's accuracy (%)	68.13	77.30

In table (5.10) performance of FCM-S was tested for untrained classes when class 2 i.e. agriculture field with crop was not considered. The overall accuracy obtained for untrained classes was 93.03% and without untrained classes the overall accuracy for FCM-S was 85.72%. But the fuzzy user's accuracy has decreased significantly if untrained class has been present in FCM-S classification. This means that in presence of untrained class the accuracy for each class on classified output has decreased as compared to the reference class.

5.6. Performance of FCM DA-MRF for untrained classes

In this section performance of FCM DA-MRF has been checked for the untrained classes. For this purpose FCM DA-MRF (H3) is taken where class 2 i.e. agriculture field with crop was remain untrained and fuzzy accuracy measure FERM was calculated as given in table (5.11). In table (5.11) performance of FCM DA-MRF was tested for untrained classes when class 2 i.e. agriculture field with crop was not considered. The overall accuracy obtained for untrained classes was 94.86% and without untrained classes the overall accuracy for FCM DA-MRF was 87.32 %. Similar result like FCM-S was found that fuzzy user's accuracy has been decreased significantly if untrained class had been present in FCM DA-MRF classification. This means that in presence of untrained class the accuracy for each class on classified images has decreased as compared to the reference class.

Table 5.11: Accuracy assessment report (FERM) of FCM DA-MRF (H3) classification for LISS-III image of Resourcesat-1 with LISS-IV as a reference image while class 2 (Agriculture field with crop) was not considered

Accuracy assessment method	Untrained(not considered agriculture field with crop)	Trained
Fuzzy user's accuracy (%)		
Dry agriculture field without crop	60.47	72.97
Moist agriculture field without crop	33.26	40.86
Eucalyptus plantation	59.85	70.65
Sal forest	36.28	47.74
Water	86.64	90.54
Average user's accuracy (%)	55.30	59.76

In figure (5.12) average user's accuracy has been compared for different classifiers with untrained class and without untrained class. For all the cases the average user's accuracy decreases when untrained class is present in the classifiers. In presence of untrained class the user's accuracy was decreased 10.63%, 9.17%, and 4.46% for FCM, FCM-S and FCM DA-MRF respectively.

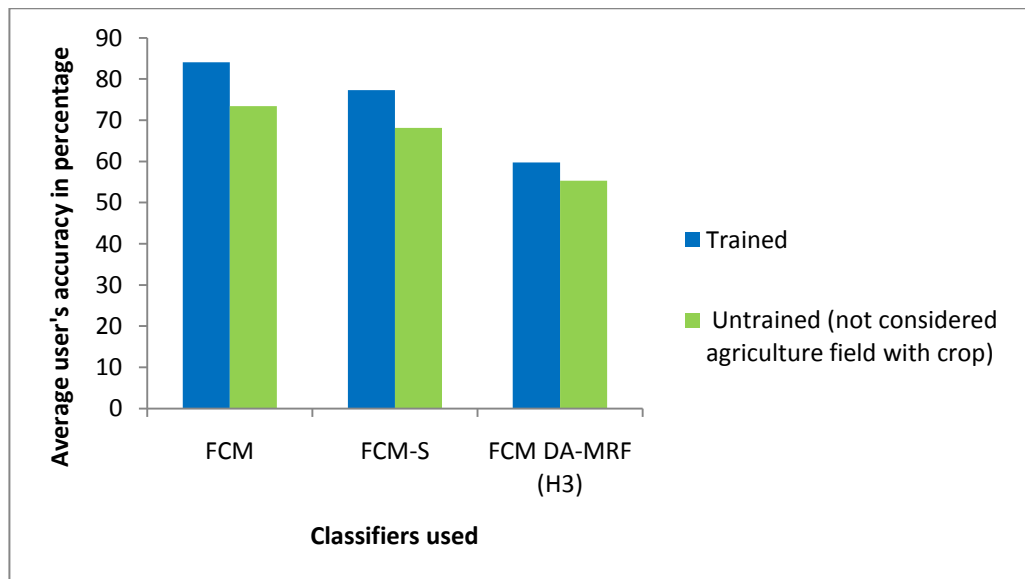


Figure 5.12: Comparison of average user's accuracy of different classifiers for LISS-III image from Resourcesat-1

5.7. Entropy measure of classified output

As explained in chapter 5, the entropy value was calculated for the best classified output of different classifiers to measure the uncertainty associated with the results as given in table (5.12).

Table 5.12: Comparison of entropy values of classified output

Classifiers	Entropy values
FCM	1.419
FCS-S	1.371
FCM DA-MRF(H1)	1.419
FCM DA-MRF(H2)	1.322
FCM DA-MRF(H3)	1.322
FCM DA-MRF(H4)	1.099

From table (5.12) it was observed that the entropy values were less in FCM-S and FCM DA-MRF in comparison to FCM. It has been noticed from table (5.12), that among the DA models, FCM DA-MRF (H4) has the lowest entropy. So it can be concluded that the classified output from FCM DA-MRF has less uncertainty as compared to FCM and among the DA models, FCM DA-MRF (H4) was less affected by uncertainty.

6. Discussion

The achieved results have been discussed in this chapter. In this research work a new method was introduced for fuzzy based classifier based on discontinuity adaptive MRF models. The applicability of discontinuity adaptive MRF models has been discussed in detail. Performances of the developed classifiers were discussed in term of classification accuracy as well.

The smoothness parameter (λ) has been estimated for MRF models in this research work as explained in section 5.1, chapter 5. The value of λ ranges between 0 and 1. It was found that the value of λ changes across the spatial resolution of images. For coarser resolution image the value of λ was higher whereas for fine resolution image the value of λ was low. It implies that for coarser resolution image the value of λ is higher because of the low variability in the image. In this study for AWiFS image with 60m spatial resolution and for LISS-IV image with 5m spatial resolution the estimated λ value for FCM-S was 0.9 and 0.7 respectively, which supports the conclusion for changes of λ . Another aspect of λ value has been explored in this research work that the optimum λ value for an image remains same regardless the radiometric accuracy of an image. The λ value has been optimized for both the Resourcesat-1 and Resourcesat-2 dataset. The radiometric accuracy was improved from 7 bits to 10 bits for LISS-III and LISS-IV and 10 bits to 12 bits for AWiFS in Resourcesat-2 as compared to Resourcesat-1. For both the Resourcesat-1 and Resourcesat-2 the estimated parameter value of λ , β and γ were found same. It suggests that the optimal λ value is invariant for radiometric accuracy in contextual image classification.

The accuracy of the classified output has been assessed using the fuzzy error matrix as provided in chapter 5. It has been found that due to incorporation of contextual information in FCM the classifier was spectrally as well as spatially consistent and 0.5% to 5% overall accuracy has been increased. The FCM classifier only takes spectral properties for classification but due to incorporation of spatial contextual information it also consider the spatial properties of the image and it increases the overall classification accuracy.

To incorporate the spatial contextual information with FCM, smoothness prior and four DA-MRF models have been used. From the accuracy assessment results in chapter 5, it has been noticed that using DA-MRF models 1.5% to 6% overall accuracy increased in comparison to smoothness prior. As explained in chapter 3, the interactions among the pixels are constant everywhere in smoothness prior model and the smoothing strength is proportional to $|\eta|$. This is why the FCM-S leads to over smoothing at edges where η is infinite. Thus adding the contextual information using smoothness prior, leads to over smoothing at the edges. Therefore FCM-S does not increase the classification accuracy. It concludes that while incorporating spatial contextual information with FCM, DA-MRF models should use for more accurate result.

The developed classifier was tested both on Resourcesat-1 and Resourcesat-2 datasets. It has been observed that due to improvement of radiometric accuracy, 0.5% to 8% of contextual classification accuracy has been achieved for Resourcesat-2. The radiometric accuracy also effect on the visual appearance on the classified output. In Resourcesat-2, the land cover classes were more clearly visible and well separated from other classes in comparison to Resourcesat-1.

For checking the preservation of edges for classified output, mean and variance method has been used as explained in section 3.12, chapter 3. The edges were checked pixel by pixel for all the classified output of AWiFS and LISS-III image. From the experimental results as presented in chapter 5, it was observed that the used method was effective for inspection of preservation of edges. As mentioned in [5] the DA-MRF models should preserve the edges whereas smoothness prior leads to over smoothing. From the results obtained by edge verification method by mean and variance (chapter 5), it was found that the DA-MRF models preserved the edges more correctly with the high mean difference and low variance than the smoothness prior. It justifies the effective inspection of preservation of edges by mean and variance method.

The preservation of edge has been checked for all the classifiers using mean and variance method for AWiFS and LISS-III image as provided in chapter 5. It has been found that the FCM DA-MRF preserves the edges correctly whereas FCM-S was unable to preserve the edges. It also has been found that preserving the edges the classification accuracy of 1.5% to 6% was improved for FCM DA-MRF (H3) as compared to FCM-S. It concludes that while using contextual classification it is very important to preserve the edges to avoid the over smoothing on the classified output.

The FCM-S and FCM DA-MRF models have been compared. It has been found that FCM DA-MRF (H3) provides the highest classification accuracy for both the AWiFS and LISS-III images as seen in chapter 5. The FCM DA-MRF (H3) performs better than the other models because of the following two reasons:

- In FCM DA-MRF (H3), η is the difference between target pixels membership value and its neighboring pixels membership value in a neighborhood window. This DA model allows smoothing strength increases monotonically as η increases within the neighborhood window. Outside the window, the smoothing strength decreases as η increases and becomes zero as $\eta \rightarrow \infty$, whereas in FCM-S, it allows boundless smoothing when $\eta \rightarrow \infty$ [5].
- At homogeneous classes, when $\eta = 0$, the FCM DA-MRF (H3) applies zero smoothing and it controls the over smoothing.

Among the DA-MRF models, the first three DA-MRF models as mentioned in equation (3.10)-(3.12) behave in a similar way to the smoothness prior model when $\frac{\eta^2}{\gamma} \ll 1$ or $\eta^2 \ll 1$ as given in [51]. From the power series expansion of $g_\gamma(\eta)$ in equation (3.10)-(3.12), it can be seen that when η^2/γ is sufficiently small, the DA-MRF models in (3.10)-(3.12) behave similar like

smoothness prior model. So the FCM DA-MRF (H4) also provides higher accuracy than FCM DA-MRF (H1) and FCM DA-MRF (H2).

The developed contextual classifier has been tested for untrained classes as explained in chapter 5. Land cover class 2 i.e. Agriculture field with crop was considered during the classification process of LISS-III images by FCM-S and FCM DA-MRF (H3). To measure the accuracy for untrained class, mean value of a known class was not provided to the classifier during the classification process but for the reference data all the classes were considered. Therefore fuzzy user's accuracy has been considered because the fuzzy user's accuracy implies the accuracy of classified images. From the results as explained in chapter 5, it has been found that in presence of untrained class the accuracy of classified output decreased significantly for all the DA-MRF models. Also the FCM, FCM-S and FCM DA-MRF (H3) have been tested and their results were compared for untrained class. It has been found that the FCM DA-MRF (H3) was less affected in presence of untrained classes in comparison to FCM and FCM-S.

From the entropy values of best classified output, it has been found that the FCM DA-MRF has less entropy in comparison to FCM and FCM-S. Among the DA-MRF models, FCM DA-MRF (H4) has minimum entropy. It indicates that FCM DA-MRF (H4) was less affected by uncertainty. This uncertainty results are independent of the reference dataset and it is an absolute measure of uncertainty of the classified output.

The FCM DA-MRF (H3) gives better accuracy than the fuzzy based classifiers, by including spatial contextual information and preserving the edges. Thus, FCM DA-MRF (H3) can be used to generate spectrally and spatial consistent thematic maps which preserves the edges.

7. Conclusion and recommendations

This chapter presents the conclusion and further recommendations for future research. In section 7.1 conclusion and in section 7.2 recommendations were given. Section 7.1 further divided as 7.1.1 to answer the research questions and 7.1.2 for further conclusions.

7.1. Conclusion

The main objective of this research work was to develop a sub-pixel classifier for classifying moderate and coarse spatial resolution multi-spectral dataset using FCM and DA-MRF models. Another objective was to study the four DA-MRF models for FCM. The efficiency for DA-MRF models has been discussed in chapter 6. In this research work a method was developed incorporating spatial contextual information in FCM using DA-MRF models which preserves the edges.

7.1.1 Answers to the research questions

Research question 1. How can spatial contextual information be incorporated into an FCM classification when DA-MRF models are to be used?

Answer: The answer of this research question has been the objective function developed and mentioned in section 3.9 chapter 3. In equation (3.20), the FCM with smoothness prior and in equation (3.21) - (3.24) FCM with DA-MRF models were given. The formulated equations were applied on the used dataset for this research. Also, the output images and their accuracy assessment results were discussed in chapter 6.

From the results and discussions (chapter 5 and 6) it can be concluded that:

- The proposed method is one of the way by which spatial contextual information can be added with FCM for sub-pixel classification.
- Incorporating spatial contextual information in FCM using DA-MRF models improves the classification accuracy by 0.5% to 5%.
- DA-MRF models with FCM preserves the edges which improves the overall accuracy of the classifier.

Research question 2. How should the FCM objective function be formulated to allow incorporation of context using DA-MRF models?

Answer: The answer to this research question was mentioned in section 3.9, chapter 3. The formulated objective functions to incorporate context by DA-MRF models has been provided in equations (3.21) - (3.24).

Research question 3. Which is a best DA-MRF model for a specific FCM?

Answer: From results and discussion (chapter 5 and 6) it has been found and discussed that FCM DA-MRF (H3) provides the highest overall accuracy and also preserves the edge and it can be concluded that DA-MRF (H3) is best suitable for FCM contextual classifier.

Research question 4. What is the accuracy of the FCM adjusted with DA-MRF model as compared to FCM?

Answer: The accuracy measure has been explained in chapter 3. As stated earlier (chapter 5) the improvement in accuracy of 0.5% to 5% has been observed for DA-MRF model as compared to FCM.

Research question 5. How much does an FCM DA-MRF model improve in terms of classification as compared to FCM with a smoothness prior MRF model?

Answer: In chapter 5, the accuracy assessment of FCM DA-MRF and FCM-S has been presented. It has been found that 1.5% to 6% improves the accuracy for FCM DA-MRF as compared to FCM with smoothness prior.

Research question 6. How does FCM DA-MRF perform in case of untrained classes?

Answer: FCM-S and FCM-DA was examined for untrained classes. Fuzzy accuracy measure FERM was calculated for FCM, FCM-S and FCM DA-MRF and from the results as given in section 5.5 and 5.6, chapter 5, it has been noticed that the FCM DA-MRF classifier was less affected than the FCM and FCM-S in presence of untrained classes.

7.1.2 Further conclusions

- The value of λ for LISS-IV and LISS-III was 0.6 and 0.9 respectively. Thus it can be concluded that the role of spatial contextual information was less in coarser resolution image whereas for finer resolution image the role of spatial contextual information increases.
- From the results of accuracy assessment for AWiFS and LISS-III image it was found that for LISS-III image FCM-S and FCM DA-MRF perform better as compared to that of FCM for AWiFS image. It means that as spatial resolution of the image becomes finer spatial context increases. It also observed that using DA-MRF model the accuracy was further improved for LISS-III image as compared to AWiFS image and DA-MRF models were used to preserve the edges. Thus it can be concluded that if spatial resolution becomes finer the discontinuities increases and it becomes essential to preserve the edge.
- It has been found from the accuracy assessment of AWiFS and LISS-III images that FCM DA-MRF (H3) performs better in case of coarse and moderate resolution images among all other DA-MRF models. It also preserves the discontinuities for the coarse and moderate spatial resolution image.
- From the results of accuracy assessment of Resourcesat-1 and Resourcesat-2 it has been found that if the radiometric accuracy is increased then the contextual classification accuracy is also increased by 0.5% to 8%.
- FCM DA-MRF classifiers were less affected in presence of untrained classes in comparison to FCM-S and FCM.
- The entropy values were calculated for the classified output of FCM, FCM-S and FCM-DA, and it was found that the uncertainty in the classified results were less in FCM DA-MRF models as compared to FCM and FCM-S.

7.2. Recommendations

To address the limitations, the following suggestions were provided for future research.

- Parameter estimation may be conducted with other methods also. Presently there are no standard methods available for parameter estimation. A comparative study can be conducted for all the available and possible methods to find out the best method for parameter estimation.
- The developed classification methods were tested in supervised approach. It can be tested in unsupervised approach also.
- For energy minimization instead of simulated annealing other methods may be tested. As per [4] Maximizing of the Posterior Marginals (MPM) is computationally fast, thus this can also be used.
- DA-MRF models may also be studied for other classification technique such as Support vector machine (SVM), Linear Mixture Modeling (LMM) etc.

List of references

- [1] L. A. Zadeh, "Fuzzy sets," *Information and control*, vol. 8, pp. 338–353, 1965.
- [2] J. C. Bezdek, R. Ehrlich, and W. Full, "FCM: the fuzzy c-means clustering algorithm," *Computers & Geosciences*, vol. 10, no. 2–3, pp. 191–203, 1984.
- [3] S. Geman and D. Geman, "Stochastic Relaxation, Gibbs Distributions, and the Bayesian Restoration of Images," *IEEE Transactions on Pattern Analysis and Machine Intelligence*, vol. PAMI-6, no. 6, pp. 721–741, Nov. 1984.
- [4] A. H. S. Solberg, T. Taxt, and A. K. Jain, "A Markov random field model for classification of multisource satellite imagery," *IEEE Transactions on Geoscience and Remote Sensing*, vol. 34, no. 1, pp. 100–113, Jan. 1996.
- [5] S. Z. Li, *Markov random fields modeling in image analysis: e-book*, Third edition. London: Springer, 2009.
- [6] B. Tso and P. M. Mather, *Classification methods for remotely sensed data*, Second edition. Boca Raton: CRC, 2009.
- [7] S. Z. Li, "On discontinuity-adaptive smoothness priors in computer vision," *IEEE Transactions on Pattern Analysis and Machine Intelligence*, vol. 17, no. 6, pp. 576–586, Jun. 1995.
- [8] J.-C. Pinoli and J. Debayle, "General Adaptive Neighborhood Mathematical Morphology," in *2009 16th IEEE International Conference on Image Processing (ICIP)*, 2009, pp. 2249–2252.
- [9] E. Binaghi, P. A. Brivio, P. Ghezzi, and A. Rampini, "A fuzzy set-based accuracy assessment of soft classification," *Pattern Recognition Letters*, vol. 20, no. 9, pp. 935–948, 1999.
- [10] J. L. Silván-Cárdenas and L. Wang, "Sub-pixel confusion–uncertainty matrix for assessing soft classifications," *Remote Sensing of Environment*, vol. 112, no. 3, pp. 1081–1095, 2008.
- [11] F. Wang, "Fuzzy supervised classification of remote sensing images," *IEEE Transactions on Geoscience and Remote Sensing*, vol. 28, no. 2, pp. 194–201, Mar. 1990.
- [12] J. Zhang and G. M. Foody, "A fuzzy classification of sub-urban land cover from remotely sensed imagery," *International Journal of Remote Sensing*, vol. 19, no. 14, pp. 2721–2738, Jan. 1998.
- [13] F. Okeke and A. Karnieli, "Methods for fuzzy classification and accuracy assessment of historical aerial photographs for vegetation change analyses. Part I: Algorithm development," *International journal of remote sensing*, vol. 27, no. 1, pp. 153–176, 2006.
- [14] S. R. Kannan, R. Devi, S. Ramathilagam, and K. Takezawa, "Effective FCM noise clustering algorithms in medical images," *Computers in Biology and Medicine*, vol. 43, no. 2, pp. 73–83, Feb. 2013.
- [15] N. S. Lucas, S. Shanmugam, and M. Barnsley, "Sub-pixel habitat mapping of a costal dune ecosystem," *Applied Geography*, vol. 22, no. 3, pp. 253–270, Jul. 2002.
- [16] G. M. FOODY, "Approaches for the production and evaluation of fuzzy land cover classifications from remotely-sensed data," *International Journal of Remote Sensing*, vol. 17, no. 7, pp. 1317–1340, May 1996.
- [17] J. Zhang and G. M. Foody, "Fully-fuzzy supervised classification of sub-urban land cover from remotely sensed imagery: Statistical and artificial neural network approaches," *International Journal of Remote Sensing*, vol. 22, no. 4, pp. 615–628, Jan. 2001.
- [18] Q. Wang, Q. Zhang, and W. Zhou, "Study on Remote Sensing Image Segmentation Based on ACA–FCM," *Physics Procedia*, vol. 33, no. 0, pp. 1286–1291, 2012.
- [19] L. Bastin, "Comparison of fuzzy c-means classification, linear mixture modelling and MLC probabilities as tools for unmixing coarse pixels," *International Journal of Remote Sensing*, vol. 18, no. 17, pp. 3629–3648, Nov. 1997.
- [20] M. A. Ibrahim, M. K. Arora, and S. K. Ghosh, "Estimating and accommodating uncertainty through the soft classification of remote sensing data," *International Journal of Remote Sensing*, vol. 26, no. 14, pp. 2995–3007, Jul. 2005.

- [21] D. Pham, "Spatial Models for Fuzzy Clustering," *Computer Vision and Image Understanding*, vol. 84, no. 2, pp. 285–297, Nov. 2001.
- [22] F. Melgani and S. B. Serpico, "A Markov random field approach to spatio-temporal contextual image classification," *Geoscience and Remote Sensing, IEEE Transactions on*, vol. 41, no. 11, pp. 2478–2487, Nov. 2003.
- [23] B. Tso and R. C. Olsen, "A contextual classification scheme based on MRF model with improved parameter estimation and multiscale fuzzy line process," *Remote Sensing of Environment*, vol. 97, no. 1, pp. 127–136, Jul. 2005.
- [24] T. Kasetkasem, M. K. Arora, and P. K. Varshney, "Super-resolution land cover mapping using a Markov random field based approach," *Remote Sensing of Environment*, vol. 96, no. 3–4, pp. 302–314, Jun. 2005.
- [25] G. Moser and S. B. Serpico, "Contextual remote-sensing image classification by support vector machines and Markov random fields," *Geoscience and Remote Sensing Symposium (IGARSS), 2010 IEEE International*, pp. 3728–3731, 25.
- [26] S. Z. Li, "Discontinuous mrf prior and robust statistics: a comparative study," *Image and Vision Computing*, vol. 13, no. 3, pp. 227–233, 1995.
- [27] P. C. Smits and S. G. Dellepiane, "Discontinuity adaptive MRF model for remote sensing image analysis," in *Geoscience and Remote Sensing, 1997. IGARSS '97. Remote Sensing - A Scientific Vision for Sustainable Development., 1997 IEEE International*, 1997, vol. 2, pp. 907–909 vol.2.
- [28] P. C. Smits and S. Dellepiane, "Information fusion in a Markov random field-based image segmentation approach using adaptive neighbourhoods," in *Pattern Recognition, 1996., Proceedings of the 13th International Conference on*, 1996, vol. 2, pp. 570–575.
- [29] M. R. P. Homem, A. L. D. Martins, and N. D. A. Mascarenhas, "Super-Resolution Image Reconstruction using the Discontinuity Adaptive ICM."
- [30] D.-J. Kang and K.-S. Roh, "A discontinuity adaptive Markov model for color image smoothing," *Image and Vision Computing*, vol. 19, no. 6, pp. 369–379, Apr. 2001.
- [31] J. Debayle and J. C. Pinoli, "General adaptive neighborhood image processing," *Journal of Mathematical Imaging and Vision*, vol. 25, no. 2, pp. 245–266, 2006.
- [32] R. G. Pontius Jr and M. L. Cheuk, "A generalized cross tabulation matrix to compare soft classified maps at multiple resolutions," *International Journal of Geographical Information Science*, vol. 20, no. 1, pp. 1–30, 2006.
- [33] H. Dehghan and H. Ghassemian, "Measurement of uncertainty by the entropy: application to the classification of MSS data," *International journal of remote sensing*, vol. 27, no. 18, pp. 4005–4014, 2006.
- [34] A. Kumar and V. K. Dadhwal, "Entropy-based fuzzy classification parameter optimization using uncertainty variation across spatial resolution," *Journal of the Indian Society of Remote Sensing*, vol. 38, no. 2, pp. 179–192, 2010.
- [35] Q. Jackson and D. A. Landgrebe, "Adaptive Bayesian contextual classification based on Markov random fields," *IEEE Transactions on Geoscience and Remote Sensing*, vol. 40, no. 11, pp. 2454 – 2463, Nov. 2002.
- [36] S. Magnussen, P. Boudewyn, and M. Wolder, "Contextual classification of Landsat TM images to forest inventory cover types," *International Journal of Remote Sensing*, vol. 25, no. 12, pp. 2421–2440, 2004.
- [37] J. Besag, "Spatial interaction and the statistical analysis of lattice systems," *Journal of the Royal Statistical Society. Series B (Methodological)*, pp. 192–236, 1974.
- [38] W. E. L. Grimson, *From images to surfaces: A computational study of the human early visual system*, vol. 4. 1981.
- [39] B. K. P. Horn and B. G. Schunck, "Determining optical flow," *Artificial intelligence*, vol. 17, no. 1, pp. 185–203, 1981.

- [40] A. Dutta, "Fuzzy c-means classification of multispectral data incorporation spatial contextual information," ITC, Enschede, 2009.
- [41] S. Chawla, "Possibilistic c - means - spatial contextual information based sub - pixel classification approach for multi - spectral data," University of Twente Faculty of Geo-Information and Earth Observation (ITC), Enschede, 2010.
- [42] N. Metropolis, A. W. Rosenbluth, M. N. Rosenbluth, A. H. Teller, and E. Teller, "Equation of state calculations by fast computing machines," *The journal of chemical physics*, vol. 21, p. 1087, 1953.
- [43] H. G. Kitaw, "Image pan-sharpening with Markov random field and simulated annealing," 2007.
- [44] W. Wen and A. Xia, "Verifying edges for visual inspection purposes," *Pattern recognition letters*, vol. 20, no. 3, pp. 315–328, 1999.
- [45] "Welcome To ISRO :: Satellites :: Earth Observation Satellite :: RESOURCESAT-2." [Online]. Available: <http://www.isro.org/satellites/resourcesat-2.aspx>. [Accessed: 08-Jan-2013].
- [46] N. R. Pal and J. C. Bezdek, "On cluster validity for the fuzzy c-means model," *Fuzzy Systems, IEEE Transactions on*, vol. 3, no. 3, pp. 370–379, 1995.
- [47] C. F. Chen and J. M. Lee, "The validity measurement of fuzzy c-means classifier for remotely sensed images," in *Paper presented at the 22nd Asian Conference on Remote Sensing*, 2001, vol. 5, p. 9.
- [48] A. Kumar, S. K. Ghosh, and V. K. Dadhwal, "Sub-pixel land cover mapping: SMIC system," *ISPRS Int. Sym. "Geospatial Databases for Sustainable Development"*, Goa, India, 2006.
- [49] R. G. Congalton, "A review of assessing the accuracy of classifications of remotely sensed data," *Remote sensing of Environment*, vol. 37, no. 1, pp. 35–46, 1991.
- [50] G. M. Foody, "Estimation of sub-pixel land cover composition in the presence of untrained classes," *Computers & Geosciences*, vol. 26, no. 4, pp. 469–478, 2000.
- [51] S. Z. Li, "Reconstruction without discontinuities," in *Computer Vision, 1990. Proceedings, Third International Conference on*, 1990, pp. 709–712.
- [52] P. Dulyakarn and Y. Rangsanteri, "Fuzzy c-means clustering using spatial information with application to remote sensing," in *Paper presented at the 22nd Asian Conference on Remote Sensing*, 2001, vol. 5, p. 9.

Appendix A

A1. Fuzzy c-Means algorithm

This section explains the theory of Fuzzy c-means clustering. This section also tells about ‘why’ FCM has been selected for this research work and the advantages of FCM.

A2. Fuzzy c-Means clustering approach

The Fuzzy c-means [2] method is a partitioning algorithm; it is widely used in pattern recognition. FCM partition the feature space and form the clusters. It calculates the membership values of the each pixel for different land cover classes. The membership values give the *degree of sharing* of a single pixel to different land cover classes with ranges between 0 and 1. Thus a pixel can belong to several land cover classes with degree of belongingness. So in FCM the clusters are not partitioned as a crisp but as a fuzzy by assigning the memberships values to the each pixel. FCM is based on the minimization of the following objective function,

$$J_m(U, V) = \sum_{j=1}^n \sum_{i=1}^c \mu_{ij}^m \|X_j - V_i\|^2, \quad 1 \leq m < \infty \quad \text{Equation (A1)}$$

Where, N is the total number of the pixels, c is the number of classes, μ_{ij} is the fuzzy membership value of the i^{th} pixel for class j , m is the weighing exponent, X_j is the vector pixel value and V_i is the mean vector of cluster j . The fuzzy membership value is calculated through an iterative optimization of equation (A1) with update of membership μ_{ij} and the cluster centers V_i [52] by:

$$\mu_{ij} = \frac{1}{\sum_{k=1}^c \left(\frac{d_{ij}}{d_{ik}} \right)^{\frac{2}{m-1}}} \quad \text{Equation (A2)}$$

$$V_i = \frac{\sum_{j=1}^N \mu_{ij}^m X_j}{\sum_{j=1}^N \mu_{ij}^m} \quad \text{Equation (A3)}$$

The iteration of (A1) will stop when $\max_j [|\mu_{ij} - \mu'_{ij}|] < \varepsilon$, where ε is a termination criterion between 0 and 1 [52].

Appendix B

B1. GUI of the tool used for accuracy assessment

Source: Kumar et al, ISRS 2008 symposium

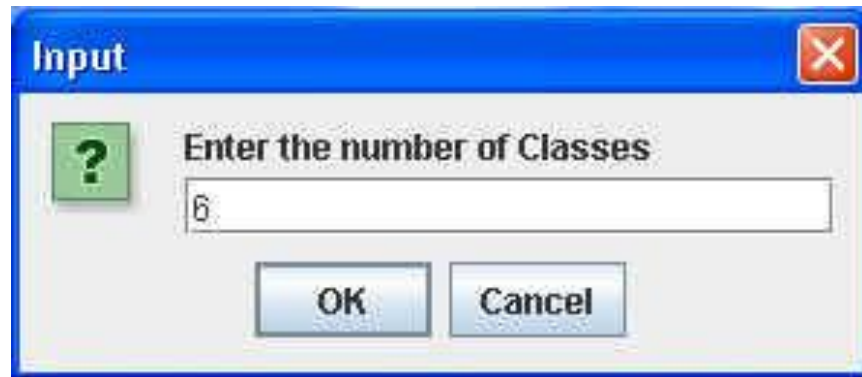


Figure B1: Total number of classes for accuracy measure



Figure B2: The spatial resolution size ratio between classified and referenced pixel

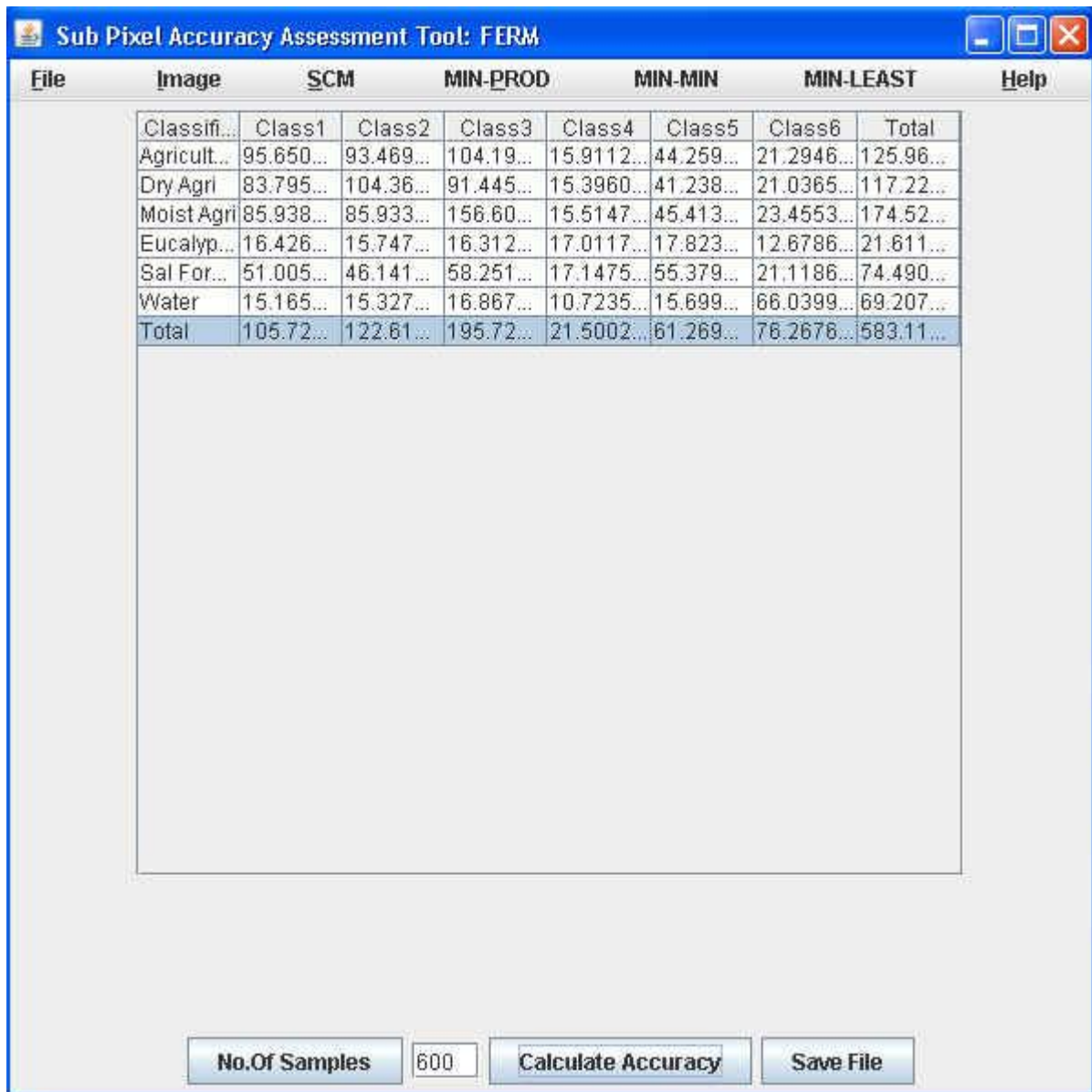


Figure B3: Fuzzy error matrix generated for the classified and reference pixels

Appendix C

Table C 1: Accuracy assessment report of FCM classification for AWiFS image of Resourcesat-1 with LISS-IV as a reference image

Accuracy assessment methods	FERM	SCM	MIN- PROD	MIN- MIN	MIN- LEAST
Fuzzy user's accuracy (%)					
Water	94.66	96.19±1.28	95.63	94.90	97.47
Agriculture field with crop	78.68	79.95±4.50	79.55	75.45	84.46
Dry agriculture field without crop	68.65	73.01±17.56	69.86	55.45	90.57
Moist agriculture field without crop	58.17	60.86±7.35	59.45	53.50	68.28
Eucalyptus plantation	84.75	91.46±1.72	91.18	89.74	93.13
Sal forest	59.47	85.83±6.03	85.60	79.79	91.86
Fuzzy producer's accuracy (%)					
Water	84.96	85.52±9.90	85.88	75.62	95.43
Agriculture field with crop	86.40	79.95±4.50	87.05	83.07	91.91
Dry agriculture field without crop	77.28	79.84±8.91	78.43	70.93	88.76
Moist agriculture field without crop	91.03	92.06±3.41	91.57	88.64	95.47
Eucalyptus plantation	68.66	70.82±5.21	69.80	65.61	76.03
Sal forest	88.26	88.96±2.77	88.78	86.19	91.74
Fuzzy overall accuracy (%)	80.89	82.25±5.17	81.75	77.07	87.43
Fuzzy Kappa	-	0.77±0.06	0.77	0.71	0.84

Table C 2: Accuracy assessment report of FCM classification for AWiFS image of Resourcesat-2 with LISS-IV as a reference image

Accuracy assessment methods	FERM	SCM	MIN- PROD	MIN- MIN	MIN- LEAST
Fuzzy user's accuracy (%)					
Water	95.85	96.29±1.69	96.08	94.60	97.98
Agriculture field with crop	76.13	77.35±3.46	77.08	73.89	80.82
Dry agriculture field without crop	83.1	84.15±2.98	72.79	70.06	77.24
Eucalyptus plantation	71.84	73.65±3.58	86.08	84.80	88.14
Sal forest	85.51	86.47±1.66	83.82	81.17	87.13
Fuzzy producer's accuracy (%)					
Water	87.82	89.05±3.55	88.5	85.50	92.60
Agriculture field with crop	79.55	80.60±2.12	80.24	78.47	82.73
Dry agriculture field without crop	83.1	89.42	88.90	86.71	92.31
Eucalyptus plantation	88.34	89.51±2.8	71.90	69.12	75.70
Sal forest	70.9	72.41±3.28	89.29	87.46	91.38
Fuzzy overall accuracy (%)	81.83	82.98±2.79	82.55	80.19	85.77
Fuzzy Kappa	-	0.78±0.03	0.78	0.75	0.82

Table C 3: Accuracy assessment report of FCM-S classification for AWiFS image of Resourcesat-1 with LISS-IV as a reference image

Accuracy assessment methods	FERM	SCM	MIN- PROD	MIN- MIN	MIN- LEAST
Fuzzy user's accuracy (%)					
Water	95.47	98.18±1.41	97.62	96.76	99.59
Agriculture field with crop	65.76	83.65±12.26	82.87	71.39	95.92
Dry agriculture field without crop	68.85	78.59±21.38	79.82	57.20	99.97
Moist agriculture field without crop	53.96	70.20±15.06	67.64	55.13	85.27
Eucalyptus plantation	86.48	95.07±3.85	95.41	91.21	98.93
Sal forest	71.69	85.33±12.67	85.26	72.66	98.00
Fuzzy producer's accuracy (%)					
Water	73.00	87.01	89.69	75.48	98.58
Agriculture field with crop	83.41	91.08±6.47	91.76	84.60	97.55
Dry agriculture field without crop	64.04	85.26±13.40	87.96	71.85	98.66
Moist agriculture field without crop	79.72	92.41±7.17	93.23	85.24	99.58
Eucalyptus plantation	66.20	78.51±14.25	75.56	64.26	92.77
Sal forest	89.67	93.61±4.24	93.88	89.36	97.85
Fuzzy overall accuracy (%)	76.04	86.62±9.96	86.54	76.65	96.58
Fuzzy Kappa	-	0.83±0.12	0.83	0.70	0.95

Table C 4: Accuracy assessment report of FCM DA-MRF (H1) classification for AWiFS image of Resourcesat-1 with LISS-IV as a reference image

Accuracy assessment methods	FERM	SCM	MIN- PROD	MIN- MIN	MIN- LEAST
Fuzzy user's accuracy (%)					
Water	95.19	96.35±1.66	95.85	94.68	98.01
Agriculture field with crop	75.94	77.16±4.51	76.85	72.65	81.68
Dry agriculture field without crop	63.04	69.13±21.13	64.24	47.99	90.27
Moist agriculture field without crop	55.59	58.59±8.13	56.86	50.46	66.73
Eucalyptus plantation	91.32	92.06±2.07	91.75	89.99	94.13
Sal forest	84.69	85.83±6.13	85.50	79.69	91.96
Fuzzy producer's accuracy (%)					
Water	78.30	78.91±10.43	79.22	68.47	89.34
Agriculture field with crop	87.83	88.92±5.22	88.48	83.69	94.14
Dry agriculture field without crop	72.45	75.65±12.21	73.66	63.44	87.87
Moist agriculture field without crop	92.16	93.13±4.23	92.68	88.90	97.37
Eucalyptus plantation	68.01	70.34±5.54	69.16	64.80	75.89
Sal forest	87.38	88.11±2.78	87.93	85.32	90.89
Fuzzy overall accuracy (%)	79.84	81.27±5.69	80.71	75.57	86.96
Fuzzy Kappa	-	0.76±0.073	0.75	0.69	0.83

Table C 5: Accuracy assessment report of FCM DA-MRF (H2) classification for AWiFS image of Resourcesat-1 with LISS-IV as a reference image

Accuracy assessment methods	FERM	SCM	MIN- PROD	MIN- MIN	MIN- LEAST
Fuzzy user's accuracy (%)					
Water	91.23	94.94±3.12	94.73	91.82	98.06
Agriculture field with crop	73.69	83.24±8.58	82.06	74.65	91.83
Dry agriculture field without crop	72.45	79.98±19.92	78.40	60.06	99.91
Moist agriculture field without crop	55.60	65.71±13.28	63.07	52.42	78.99
Eucalyptus plantation	90.79	94.68±2.05	94.74	92.63	96.73
Sal forest	79.95	86.03±10.22	85.29	75.80	96.26
Fuzzy producer's accuracy (%)					
Water	69.13	84.29±8.80	85.50	75.49	93.10
Agriculture field with crop	83.32	89.48±6.66	89.60	82.81	96.14
Dry agriculture field without crop	60.33	75.06±12.31	76.40	62.76	87.37
Moist agriculture field without crop	84.00	94.21±4.51	94.79	89.70	98.73
Eucalyptus plantation	68.35	78.73±11.41	75.82	67.31	90.14
Sal forest	87.20	90.76±3.90	91.09	86.85	94.67
Fuzzy overall accuracy (%)	76.25	85.33±8.18	84.73	77.15	93.51
Fuzzy Kappa	-	0.81±0.10	0.80	0.71	0.91

Table C 6: Accuracy assessment report of FCM DA-MRF (H3) classification for AWiFS image of Resourcesat-1 with LISS-IV as a reference image

Accuracy assessment methods	FERM	SCM	MIN- PROD	MIN- MIN	MIN- LEAST
Fuzzy user's accuracy (%)					
Water	89.57	97.75±2.0	98.07	95.69	99.80
Agriculture field with crop	37.35	76.75±21.04	75.59	55.71	97.80
Dry agriculture field without crop	62.07	82.77±17.22	86.90	65.55	100
Moist agriculture field without crop	36.15	72.94±21.71	70.74	51.23	94.66
Eucalyptus plantation	73.89	93.86±5.79	95.26	88.06	99.66
Sal forest	48.81	81.31±17.15	82.91	64.15	98.46
Fuzzy producer's accuracy (%)					
Water	87.04	87.75±10.23	90.07	77.51	97.99
Agriculture field with crop	89.92	91.23±7.58	93.56	83.64	98.81
Dry agriculture field without crop	61.39	76.46±20.82	79.46	55.63	97.29
Moist agriculture field without crop	85.62	89.03±10.57	92.38	78.46	99.60
Eucalyptus plantation	73.92	79.14±19.62	78.27	59.51	98.76
Sal forest	91.32	92.99±5.81	93.02	87.17	98.81
Fuzzy overall accuracy (%)	81.97	85.19±13.46	86.58	71.73	98.66
Fuzzy Kappa	-	0.81±0.17	0.82	0.64	0.98

Table C 7: Accuracy assessment report of FCM DA-MRF (H4) classification for AWiFS image of Resourcesat-1 with LISS-IV as a reference image

Accuracy assessment methods	FERM	SCM	MIN- PROD	MIN- MIN	MIN- LEAST
Fuzzy user's accuracy (%)					
Water	92.24	97.62±2.36	97.87	95.26	99.99
Agriculture field with crop	43.69	77.15±20.05	75.03	57.10	97.21
Dry agriculture field without crop	72.83	85.83±14.16	88.73	71.67	100
Moist agriculture field without crop	35.29	66.70±24.64	60.96	42.06	91.34
Eucalyptus plantation	81.41	94.80±4.96	95.84	89.83	99.77
Sal forest	59.47	83.55±15.82	84.16	67.73	99.37
Fuzzy producer's accuracy (%)					
Water	81.28	88.05±9.94	89.45	78.01	98.00
Agriculture field with crop	86.69	90.65±8.99	92.17	81.66	99.64
Dry agriculture field without crop	78.44	79.84±19.94	86.25	59.90	99.78
Moist agriculture field without crop	83.80	90.48±9.50	93.15	80.97	99.99
Eucalyptus plantation	70.83	79.46±18.64	77.52	60.81	98.11
Sal forest	89.24	91.82±6.82	92.19	85.00	98.64
Fuzzy overall accuracy (%)	81.71	85.33±13.31	85.83	72.01	98.65
Fuzzy Kappa	-	0.80±0.17	0.81	0.64	0.98

Table C 8: Accuracy assessment report of FCM-S classification for AWiFS image of Resourcesat-2 with LISS-IV as a reference image

Accuracy assessment methods	FERM	SCM	MIN- PROD	MIN- MIN	MIN- LEAST
Fuzzy user's accuracy (%)					
Water	95.83	97.43±1.49	97.64	95.94	98.93
Agriculture field with crop	62.70	76.59±7.72	76.60	68.86	84.32
Dry agriculture field without crop	66.55	79.81±5.79	79.13	74.02	85.61
Eucalyptus plantation	70.47	95.21±2.84	95.07	92.37	98.06
Sal forest	77.68	87.91±8.00	87.79	79.90	95.91
Fuzzy producer's accuracy (%)					
Water	88.82	91.35±5.04	92.14	86.31	96.40
Agriculture field with crop	87.31	89.49±3.73	89.7	85.76	93.22
Dry agriculture field without crop	93.41	89.89±6.00	89.65	83.89	95.89
Eucalyptus plantation	86.63	77.12±8.19	76.22	68.93	85.32
Sal forest	73.40	94.05±1.81	94.33	92.94	95.87
Fuzzy overall accuracy (%)	84.75	87.33±5.42	87.26	81.90	92.75
Fuzzy Kappa	-	0.84±0.06	0.84	0.77	0.90

Table C 9: Accuracy assessment report of FCM DA-MRF (H1) classification for AWiFS image of Resourcesat-2 with LISS-IV as a reference image

Accuracy assessment methods	FERM	SCM	MIN- PROD	MIN- MIN	MIN- LEAST
Fuzzy user's accuracy (%)					
Water	94.84	95.38±1.82	95.12	93.56	97.20
Agriculture field with crop	76.82	77.98±3.96	77.72	74.02	81.94
Dry agriculture field without crop	72.85	74.55±3.49	73.76	71.05	78.04
Eucalyptus plantation	87.84	88.76±1.95	88.39	86.81	90.72
Sal forest	82.10	83.34±3.59	82.89	79.74	86.93
Fuzzy producer's accuracy (%)					
Water	90.45	91.67±4.15	91.41	87.52	95.82
Agriculture field with crop	80.56	81.72±2.43	81.30	79.28	84.16
Dry agriculture field without crop	85.69	86.90±3.30	86.30	83.60	90.20
Eucalyptus plantation	72.58	73.99±3.31	73.52	70.68	77.30
Sal forest	88.98	89.59±2.31	89.43	87.28	91.91
Fuzzy overall accuracy (%)	82.37	83.53±3.08	83.10	80.44	86.62
Fuzzy Kappa	-	0.79±0.038	0.78	0.75	0.83

Table C 10: Accuracy assessment report of FCM DA-MRF (H2) classification for AWiFS image of Resourcesat-2 with LISS-IV as a reference image

Accuracy assessment methods	FERM	SCM	MIN- PROD	MIN- MIN	MIN- LEAST
Fuzzy user's accuracy (%)					
Water	92.85	94.52±2.89	94.67	91.62	97.42
Agriculture field with crop	73.76	80.87±6.71	80.60	74.15	87.59
Dry agriculture field without crop	73.88	78.57±4.97	78.11	73.60	83.55
Eucalyptus plantation	82.94	91.41±2.81	91.19	88.60	94.23
Sal forest	74.99	86.90±6.51	86.19	80.39	93.42
Fuzzy producer's accuracy (%)					
Water	89.99	91.57±4.58	92.31	86.98	96.15
Agriculture field with crop	80.86	83.81±4.51	83.47	79.29	88.32
Dry agriculture field without crop	83.68	88.37±4.61	87.60	83.75	92.99
Eucalyptus plantation	73.58	78.25±7.08	77.26	71.16	85.33
Sal forest	91.69	92.76±2.39	93.01	90.36	95.15
Fuzzy overall accuracy (%)	82.87	86.10±4.93	85.79	81.16	91.04
Fuzzy Kappa	-	0.82±0.06	0.82	0.76	0.88

Table C 11: Accuracy assessment report of FCM DA-MRF (H3) classification for AWiFS image of Resourcesat-2 with LISS-IV as a reference image

Accuracy assessment methods	FERM	SCM	MIN- PROD	MIN- MIN	MIN- LEAST
Fuzzy user's accuracy (%)					
Water	96.29	98.57±1.28	98.79	97.28	99.85
Agriculture field with crop	50.40	80.98±14.01	80.93	66.96	95.00
Dry agriculture field without crop	65.92	87.62±6.82	87.82	80.79	94.44
Eucalyptus plantation	62.73	90.91±6.46	91.54	84.44	97.38
Sal forest	41.98	82.03±15.01	81.80	67.01	97.05
Fuzzy producer's accuracy (%)					
Water	86.54	88.61±6.75	89.53	81.85	95.37
Agriculture field with crop	89.63	90.36±6.56	91.07	83.79	96.93
Dry agriculture field without crop	89.84	90.76±8.52	91.72	82.24	99.29
Eucalyptus plantation	79.38	81.76±13.97	80.90	67.79	95.73
Sal forest	94.37	95.71±1.80	95.85	93.91	97.51
Fuzzy overall accuracy (%)	87.02	88.43±8.47	88.97	79.99	96.87
Fuzzy Kappa	-	0.85±0.10	0.86	0.74	0.96

Table C 12: Accuracy assessment report of FCM DA-MRF (H4) classification for AWiFS image of Resourcesat-2 with LISS-IV as a reference image

Accuracy assessment methods	FERM	SCM	MIN- PROD	MIN- MIN	MIN- LEAST
Fuzzy user's accuracy (%)					
Water	93.96	96.50±3.21	97.13	93.29	99.72
Agriculture field with crop	55.82	79.56±14.13	78.49	65.43	93.69
Dry agriculture field without crop	59.70	79.25±12.05	77.22	67.20	91.30
Eucalyptus plantation	71.91	93.63±5.02	93.58	88.60	98.65
Sal forest	50.99	84.77±14.09	84.22	70.67	98.87
Fuzzy producer's accuracy (%)					
Water	88.63	90.45±6.49	91.40	83.95	96.94
Agriculture field with crop	81.84	86.50±10.31	86.15	76.18	96.82
Dry agriculture field without crop	82.98	88.02±10.57	87.25	77.44	98.60
Eucalyptus plantation	73.60	79.46±14.95	77.61	64.51	94.41
Sal forest	94.67	95.78±2.16	95.61	93.61	97.95
Fuzzy overall accuracy (%)	82.94	86.74±9.94	86.40	76.79	96.69
Fuzzy Kappa	-	0.83±0.12	0.82	0.70	0.95

Table C 13: Accuracy assessment report of FCM-S classification for LISS-III image of Resourcesat-1 with LISS-IV as a reference image

Accuracy assessment methods	FERM	SCM	MIN- PROD	MIN- MIN	MIN- LEAST
Fuzzy user's accuracy (%)					
Water	94.26	97.20±1.26	96.89	95.93	98.47
Agriculture field with crop	64.78	85.24±10.04	84.79	75.22	95.27
Dry agriculture field without crop	79.03	88.99±9.79	89.31	79.19	98.79
Moist agriculture field without crop	67.66	81.31±10.86	80.43	70.45	92.18
Eucalyptus plantation	84.28	96.22±3.24	96.70	92.97	99.46
Sal forest	73.80	89.65±9.14	90.07	80.51	98.79
Fuzzy producer's accuracy (%)					
Water	90.95	93.94±5.70	96.30	88.24	99.65
Agriculture field with crop	92.15	95.27±3.70	95.50	91.57	98.97
Dry agriculture field without crop	77.14	85.22±12.89	88.40	72.33	98.11
Moist agriculture field without crop	87.59	91.93±6.91	92.68	85.01	98.85
Eucalyptus plantation	76.65	84.77±9.95	82.85	74.82	94.73
Sal forest	91.47	94.12±3.54	94.35	90.58	97.67
Fuzzy overall accuracy (%)	85.72	90.70±6.82	90.85	83.87	97.53
Fuzzy Kappa	-	0.88±0.085	0.88	0.79	0.96

Table C 14: Accuracy assessment report of FCM DA-MRF (H1) classification for LISS-III image of Resourcesat-1 with LISS-IV as a reference image

Accuracy assessment methods	FERM	SCM	MIN- PROD	MIN- MIN	MIN- LEAST
Fuzzy user's accuracy (%)					
Water	95.20	96.41±1.94	95.79	94.46	98.35
Agriculture field with crop	76.21	77.60±4.51	77.37	73.09	82.12
Dry agriculture field without crop	75.10	78.21±10.99	76.37	67.21	89.21
Moist agriculture field without crop	76.79	79.07±6.43	78.10	72.64	85.51
Eucalyptus plantation	91.28	92.09±2.22	91.80	89.87	94.31
Sal forest	87.05	88.03±4.76	87.84	83.26	92.80
Fuzzy producer's accuracy (%)					
Water	89.79	89.92±6.84	90.64	83.07	96.77
Agriculture field with crop	91.14	92.10±2.84	91.74	89.25	94.94
Dry agriculture field without crop	81.80	83.31±11.86	83.11	71.44	95.17
Moist agriculture field without crop	87.37	89.25±5.71	88.24	83.53	94.97
Eucalyptus plantation	78.27	80.16±4.00	79.35	76.16	84.17
Sal forest	86.06	87.08±2.20	86.80	84.87	89.29
Fuzzy overall accuracy (%)	84.96	86.23±4.24	85.84	81.98	90.48
Fuzzy Kappa	-	0.82±0.054	0.82	0.77	0.87

Table C 15: Accuracy assessment report of FCM DA-MRF (H2) classification for LISS-III image of Resourcesat-1 with LISS-IV as a reference image

Accuracy assessment methods	FERM	SCM	MIN- PROD	MIN- MIN	MIN- LEAST
Fuzzy user's accuracy (%)					
Water	94.09	96.61±1.81	96.68	94.80	98.42
Agriculture field with crop	73.01	82.91±9.01	82.14	73.90	91.92
Dry agriculture field without crop	77.60	85.85±12.92	84.77	72.92	98.77
Moist agriculture field without crop	73.05	82.06±10.32	80.58	71.73	92.38
Eucalyptus plantation	89.86	94.34±2.84	94.31	91.49	97.19
Sal forest	81.96	88.88±8.23	88.36	80.65	97.12
Fuzzy producer's accuracy (%)					
Water	91.34	93.81±5.44	95.77	88.36	99.26
Agriculture field with crop	90.13	93.65±3.53	93.92	90.12	97.18
Dry agriculture field without crop	73.18	81.79±11.55	82.29	70.23	93.34
Moist agriculture field without crop	88.96	92.82±6.07	93.52	86.75	98.90
Eucalyptus plantation	75.54	83.72±9.54	81.33	74.17	93.26
Sal forest	86.74	90.28±4.33	90.21	85.95	94.62
Fuzzy overall accuracy (%)	83.90	89.13±6.63	88.77	82.50	95.77
Fuzzy Kappa	-	0.86±0.08	0.85	0.77	0.94

Table C 16: Accuracy assessment report of FCM DA-MRF (H3) classification for LISS-III image of Resourcesat-1 with LISS-IV as a reference image

Accuracy assessment methods	FERM	SCM	MIN- PROD	MIN- MIN	MIN- LEAST
Fuzzy user's accuracy (%)					
Water	90.54	97.71±1.82	98.06	95.88	99.93
Agriculture field with crop	35.78	78.42±19.03	76.13	59.39	97.45
Dry agriculture field without crop	72.97	90.86±9.13	92.82	81.72	100
Moist agriculture field without crop	40.86	79.85±19.92	79.58	59.93	99.77
Eucalyptus plantation	70.65	95.53±4.32	96.61	91.21	99.86
Sal forest	47.74	83.95±15.45	84.62	68.50	99.41
Fuzzy producer's accuracy (%)					
Water	95.16	94.41±5.53	96.59	88.87	99.95
Agriculture field with crop	94.24	94.28±5.46	95.37	88.81	99.74
Dry agriculture field without crop	85.16	83.78±15.19	87.84	68.58	98.97
Moist agriculture field without crop	86.43	88.94±10.06	90.47	78.88	99.01
Eucalyptus plantation	80.36	83.45±16.01	82.72	67.43	99.47
Sal forest	90.07	91.84±6.60	91.94	85.23	98.45
Fuzzy overall accuracy (%)	87.31	88.53±10.83	89.44	77.70	99.36
Fuzzy Kappa	-	0.85±0.13	0.86	0.71	0.99

Table C 17: Accuracy assessment report of FCM DA-MRF (H4) classification for LISS-III image of Resourcesat-1 with LISS-IV as a reference image

Accuracy assessment methods	FERM	SCM	MIN- PROD	MIN- MIN	MIN- LEAST
Fuzzy user's accuracy (%)					
Water	93.34	97.29±1.64	97.70	95.64	98.93
Agriculture field with crop	44.21	78.75±19.27	76.71	59.47	98.02
Dry agriculture field without crop	77.80	91.30±8.45	92.86	82.84	99.76
Moist agriculture field without crop	48.19	77.86±20.32	77.11	57.53	98.18
Eucalyptus plantation	77.89	94.82±4.92	95.90	89.90	99.74
Sal forest	59.36	85.03±14.60	86.16	70.42	99.64
Fuzzy producer's accuracy (%)					
Water	95.71	95.05±4.87	97.25	90.17	99.93
Agriculture field with crop	89.94	92.77±6.46	93.79	86.31	99.23
Dry agriculture field without crop	80.05	80.32±18.70	84.95	61.61	99.02
Moist agriculture field without crop	87.41	90.08±8.80	92.13	81.28	98.88
Eucalyptus plantation	77.29	82.66±16.48	81.93	66.18	99.15
Sal forest	87.01	90.97±7.57	90.81	83.39	98.55
Fuzzy overall accuracy (%)	85.00	87.98±11.18	88.94	76.80	99.17
Fuzzy Kappa	-	0.84	0.85	0.70	0.98

Table C 18: Accuracy assessment report of FCM-S classification for LISS-III image of Resourcesat-2 with LISS-IV as a reference image

Accuracy assessment methods	FERM	SCM	MIN- PROD	MIN- MIN	MIN- LEAST
Fuzzy user's accuracy (%)					
Water	96.29	97.65±2.27	97.97	95.38	99.93
Agriculture field with crop	70.27	84.28±6.98	84.75	77.30	91.27
Dry agriculture field without crop	80.09	86.52±2.84	85.98	83.67	89.36
Eucalyptus plantation	70.99	94.39±3.93	94.06	90.45	98.32
Sal forest	65.90	87.65±7.36	87.90	80.28	95.02
Fuzzy producer's accuracy (%)					
Water	95.19	96.05±3.16	96.55	92.88	99.21
Agriculture field with crop	83.47	88.57±4.57	88.34	84.00	93.15
Dry agriculture field without crop	80.34	88.60±8.45	88.90	80.14	97.06
Eucalyptus plantation	79.59	84.46±5.26	83.92	79.19	89.73
Sal forest	94.05	95.67±1.68	95.96	93.98	97.35
Fuzzy overall accuracy (%)	86.22	90.42±4.70	90.50	85.71	95.12
Fuzzy Kappa	-	0.87±0.059	0.88	0.82	0.93

Table C 19: Accuracy assessment report of FCM DA-MRF (H1) classification for LISS-III image of Resourcesat-2 with LISS-IV as a reference image

Accuracy assessment methods	FERM	SCM	MIN- PROD	MIN- MIN	MIN- LEAST
Fuzzy user's accuracy (%)					
Water	95.27	95.97±2.75	95.73	93.21	98.72
Agriculture field with crop	82.57	83.74±3.82	83.42	79.92	87.56
Dry agriculture field without crop	77.63	79.13±2.46	78.47	76.67	81.59
Eucalyptus plantation	85.71	86.63±1.96	86.28	84.66	88.60
Sal forest	82.03	83.17±3.81	82.85	79.36	86.98
Fuzzy producer's accuracy (%)					
Water	92.44	93.37±3.67	92.97	89.69	97.05
Agriculture field with crop	81.01	82.20±2.22	81.79	79.97	84.42
Dry agriculture field without crop	83.76	85.38±5.10	84.60	80.28	90.48
Eucalyptus plantation	78.76	80.07±3.16	79.68	76.90	83.24
Sal forest	88.11	88.67±1.42	88.58	87.25	90.09
Fuzzy overall accuracy (%)	83.86	84.98±2.98	84.60	82.00	87.97
Fuzzy Kappa	-	0.80±0.03	0.80	0.77	0.84

Table C 20: Accuracy assessment report of FCM DA-MRF (H2) classification for LISS-III image of Resourcesat-2 with LISS-IV as a reference image

Accuracy assessment methods	FERM	SCM	MIN- PROD	MIN- MIN	MIN- LEAST
Fuzzy user's accuracy (%)					
Water	95.02	95.94 \pm 3.10	96.15	92.84	99.04
Agriculture field with crop	78.30	84.52 \pm 5.79	85.00	78.72	90.32
Dry agriculture field without crop	82.20	85.03 \pm 2.89	85.01	82.13	87.93
Eucalyptus plantation	85.86	93.99 \pm 2.91	93.67	91.08	96.90
Sal forest	76.27	87.49 \pm 6.91	87.49	80.58	94.41
Fuzzy producer's accuracy (%)					
Water	93.37	94.33 \pm 3.62	95.24	90.70	97.96
Agriculture field with crop	78.81	86.61 \pm 4.21	86.49	82.40	90.83
Dry agriculture field without crop	81.19	88.10 \pm 6.50	88.18	81.59	94.60
Eucalyptus plantation	78.45	85.03 \pm 2.89	84.56	79.87	90.16
Sal forest	92.45	95.30 \pm 1.61	95.67	93.69	96.92
Fuzzy overall accuracy (%)	83.76	89.24 \pm 4.39	89.32	84.84	93.63
Fuzzy Kappa	-	0.86 \pm 0.05	0.86	0.80	0.91

Table C 21: Accuracy assessment report of FCM DA-MRF (H3) classification for LISS-III image of Resourcesat-2 with LISS-IV as a reference image

Accuracy assessment methods	FERM	SCM	MIN- PROD	MIN- MIN	MIN- LEAST
Fuzzy user's accuracy (%)					
Water	96.16	98.48±1.51	98.77	96.97	100
Agriculture field with crop	54.55	82.97±13.45	83.36	69.52	96.42
Dry agriculture field without crop	72.30	90.62±5.34	90.77	85.28	95.96
Eucalyptus plantation	62.92	93.42±5.98	93.46	87.43	99.40
Sal forest	44.91	83.14±14.85	82.03	68.28	98.00
Fuzzy producer's accuracy (%)					
Water	92.54	93.88±5.21	94.79	88.76	99.00
Agriculture field with crop	85.01	87.72±9.80	87.55	77.91	97.53
Dry agriculture field without crop	89.48	91.72±8.18	92.39	83.53	99.91
Eucalyptus plantation	79.93	83.96±12.29	83.21	71.67	96.26
Sal forest	95.91	96.76±1.37	96.92	95.38	98.14
Fuzzy overall accuracy (%)	87.85	90.12±8.01	90.42	82.10	98.14
Fuzzy Kappa	-	0.87±0.10	0.87	0.77	0.97

Table C 22: Accuracy assessment report of FCM DA-MRF (H4) classification for LISS-III image of Resourcesat-2 with LISS-IV as a reference image

Accuracy assessment methods	FERM	SCM	MIN- PROD	MIN- MIN	MIN- LEAST
Fuzzy user's accuracy (%)					
Water	95.26	97.61±2.02	98.02	95.58	99.64
Agriculture field with crop	61.68	84.27±13.16	84.36	71.10	97.44
Dry agriculture field without crop	77.25	91.09±5.05	91.03	86.03	96.15
Eucalyptus plantation	67.60	92.04±6.30	92.30	85.73	98.35
Sal forest	56.34	85.55±13.39	85.21	72.16	98.94
Fuzzy producer's accuracy (%)					
Water	91.81	94.10±4.97	95.36	89.13	99.07
Agriculture field with crop	78.96	88.09±9.40	87.65	78.68	97.49
Dry agriculture field without crop	86.31	90.81±8.66	91.48	82.14	99.48
Eucalyptus plantation	79.15	85.98±11.20	85.39	74.77	97.19
Sal forest	91.89	94.33±2.87	94.62	91.46	97.21
Fuzzy overall accuracy (%)	85.29	90.31±7.81	90.65	82.50	98.12
Fuzzy Kappa	-	0.87	0.88	0.78	0.97

Appendix D

Publications related to this study:

- a) M.Singha, A.kumar, and A.Stein, “Study the effect of MRF models in fuzzy based classifier”, *ISRS Symposium*, 2012, held at New Delhi, India from Dec. 5-7.
- b) M.Singha, A.kumar, and A.Stein, “Importance of DA MRF models in fuzzy based classifier” (Paper writing in progress).